PNNL-14172

Pacific Northwest
National Laboratory
Operated by Battelle for the
U.S. Department of Energy

The Impact of Humidity, Temperature and Ultraviolet Light on the Near-Field Environmental Fate of Pinacolyl Alcohol, Methyl Iodide, Methylphosphonic Dichloride (DCMP) and Thionyl Chloride Using an Environmental Wind Tunnel

C.J. Driver
Y-F. Su
R.J. Fellows
R.S. Disselkamp
T.J. Johnson
M.L. Alexander
J. Magnuson
B.A. Roberts

January 2003

Prepared for the U.S. Department of Energy
under Contract DE-AC06-76RL01830

Pacific Northwest National Laboratory
Richland, Washington 99352

DISCLAIMER

PACIFIC NORTHWEST NATIONAL LABORATORY
operated by
BATTELLE
for the
UNITED STATES DEPARTMENT OF ENERGY
under Contract DE-AC06-76RL01830

PNNL - 14172

The Impact of Humidity, Temperature and Ultraviolet Light on the Near-Field Environmental Fate of Pinacolyl Alcohol, Methyl Iodide, Methylphosphonic Dichloride (DCMP) and Thionyl Chloride Using an Environmental Wind Tunnel

C. J. Driver
Y-F. Su
R. J. Fellows
R. S. Disselkamp
T. J. Johnson
M. L. Alexander
J. Magnuson
B. A. Roberts

January 2003

Prepared for the US Department of Energy
under Contract DE-AC06-76RLO 1830

Pacific Northwest National Laboratory
Richland, Washington 99352

EXECUTIVE SUMMARY

Understanding the near-field fate of parent chemicals and their decay products (potential additional signatures) in the atmosphere provides essential information for the development of remote chemical sensors. To elucidate the near-field fate of candidate chemical signatures, selected gas phase compounds were introduced into atmospheres of varying humidity, temperature and incident light flux. These atmospheres were maintained in an environmental wind tunnel for periods typical of near-field transport scenarios. The range of humidity and temperature into which the compounds were emitted encompassed arid, temperate, and tropical values. Simulated sunlight exposure was used to evaluate the impact of time of release (daytime or nighttime) on signature composition. The rates of compound decay and evolution of transformation products under the various environmental conditions were monitored in real time. A Fourier transform infrared spectrometer (FTIR) and a gas chromatograph/mass spectrometer (GC/MS) were used to determine chemical concentration, evaluate detectability, and identify potential interferences to the detection capability.

Specifically, this report describes the initial system function tests with pinacolyl alcohol ($(CH_3)_3CCHOHCH_3$) and methyl iodide (CH_3I) and subsequent atmospheric fate experiments with methylphosphonic dichloride (DCMP) and thionyl chloride ($SOCl_2$). Test system function was evaluated using pinacolyl alcohol because as a relatively non-reactive compound, it served as a negative control for the system. Methyl iodide is a compound known to photodissociate in the atmosphere and therefore was used to evaluate the effectiveness of the test system to detect a known positive effect under specific conditions. Results from the function tests showed that sufficient vapor generation into the large volume (2400 ft^3) of the wind tunnel could be accomplished within a reasonable time period and that the operating conditions of the wind tunnel did not appear to affect the decay rate of the two initial test chemicals.

As expected, no near-field decay of pinacolyl alcohol was observed under a wide range of temperature and humidity conditions. Further, both analytical techniques could detect pinacolyl alcohol at and below field-relevant concentrations. No significant difference in the disappearance of pinacolyl alcohol from the wind tunnel atmosphere was observed when the contaminated atmosphere was illuminated with simulated sunlight. We also observed that plants exposed to pinacolyl alcohol absorbed it and then continued to outgas the absorbed compound for a period of hours after being removed from the contaminated atmosphere.

Methyl iodide similarly proved unreactive as a function of humidity and temperature. It is known to photodissociate when exposed to ultraviolet (UV) light. However, the effective exposure time of the chemical to UV light in the open loop configuration of the wind tunnel was determined to be less than that needed to simulate near-field transport in a reasonable time frame. Therefore, the system was modified to lengthen the exposure time of the chemical to simulated sunlight by closing off a portion of the wind tunnel under the UV lights and making a semi-dynamic chamber (SDC). The SDC was lined and sealed with Teflon® film to provide an inert surface for testing the selected reactive reagents. It was used for the remaining test chemicals. This system was used to evaluate the loss rate of methyl iodide under UV irradiation and showed that the compound decayed at a rate comparable to values reported in the literature. Under the lighting and concentration conditions tested, methanol appeared to be a significant photolysis decay product of the methyl iodide. At low concentrations, water vapor interfered somewhat with the quantification of methyl iodide.

The atmospheric fate of DCMP and $SOCl_2$ were also investigated in the semi-dynamic system under various conditions of temperature, humidity and lighting. Relative humidity was found to play an important role in the environmental fate of both compounds. DCMP exhibited an exponential decay rate whose lifetime was a function of the relative humidity. Compound dissociation was so rapid at high relative humidity (≥80% RH) that sufficient concentrations of the parent chemical could not be attained to permit reliable determination of the decay rate. For humidities <80%, the rate constant for hydrolysis of DCMP at 296K was determined to be $k_h = 6.0 \pm 1.9 \times 10^{-21}$ cm^3/(molecule-sec), resulting in a typical tropospheric lifetime on the order of only a few minutes due to hydrolysis. Concomitant to the decay of gas-phase DCMP, we observed the evolution of decay products, in particular HCl(g). The relationship between the relative humidity and generated HCl concentrations were complex and may be related to additional decay product reactions and/or liquid phase adsorption.

In a similar fashion, $SOCl_2$ vapor reacted rapidly with water vapor. The two major decay products of the hydrolysis were HCl(g) and SO_2(g), formed in a nearly stoichiometric ratio of 2:1. The rate constants for the hydrolysis of $SOCl_2$ at 297 K and 309 K were measured to be $5.0 \pm 1.3 \times 10^{-21}$ and $4.3 \pm 1.5 \times 10^{-21}$ cm^3/(molecule-sec), respectively. These indicate an atmospheric lifetime of less than 10 minutes for typical conditions.

This study looked at environmental conditions typical of midlatitude environmental conditions, particularly humidity. The results indicate that the near field fate (first 1500 m) of parent compounds must be considered when choosing chemical signatures for detection. Failure to do so may cause one to incorrectly identify pollution sources or inaccurately estimate their production.

CONTENTS

FIGURES

TABLES

ABBREVIATIONS, ACRONYMS, AND CHEMICAL FORMULAE

cfm	Cubic Feet per Minute
Cl_2	Chlorine (gas)
CH_3I	Methyl Iodide
CO_2	Carbon Dioxide
DCMP	Methylphosphonic Dichloride
DOE	U.S. Department of Energy
ECD	Electron Capture Detector
FID	Flame Ionization Detector
FTIR	Fourier Transform Infrared
GC	Gas Chromatography
GC-MS	Gas Chromatograph - Mass Spectrometer
HEPA	High-Efficiency Particulate Air
H_2	Hydrogen (gas)
HCl	Hydrogen Chloride
HF	Hydrogen Fluoride
H_2O	Water
HP	Hewlett-Packard
i.d.	Inside Diameter
IR	Infrared
LWC	Liquid Water Content
MF	Methyl phosphonofluoride acid
mmHg	Millimeters of Mercury (Torr)
MPA	Methylphosphonic Acid
NIST	National Institute of Standards and Technology
N_2	Nitrogen (gas)
O_2	Oxygen (gas)
OH	Hydroxyl Radical
PNNL	Pacific Northwest National Laboratory
PA	Pinacolyl Alcohol (3,3-dimethyl-2-butanol)
PAKM	Pulsed-Aliquot-Kinetic-Method
ppm	Parts Per Million (mass)
ppmV	Parts Per Million Volume
RH	Relative Humidity
SDC	Semi-Dynamic Chamber System
SAR	Structure Activity Relationships
SO_2	Sulfur Dioxide
$SOCl_2$	Thionyl Chloride
UHP	Ultra-High Purity
UV	Ultraviolet
UV/Vis	Ultraviolet/Visible

1.0 Introduction

Remote chemical detection relies on the ability of sensors to detect airborne chemical signatures from production processes. Key to successful detection and identification in the near field (defined here as within 1500 m of the point of release) is an understanding of the behavior of chemicals under local, changing environmental conditions. Chemicals entering the atmosphere are subject to not only dispersion and diffusion (transport), but also to physical and chemical processes that remove them from the air or transform them to other species (fate). Understanding the conditions that influence compound evolution in near-field time scales is thus crucial to reliable detection of pollution and to verification of a particular site as the source of that pollution. In addition, elucidating near-field fate can lead to identification of additional, more robust signatures that evolve from decay processes.

Researchers at the Pacific Northwest National Laboratory[1] use fate and transport analysis tools to predict the chemical species, concentrations, and sampling times that optimize detection opportunity (e.g. Probasco et al., 2001 a, b). Models are used because it is impossible to examine the impact of the full range of meteorological and emission scenarios on chemical concentration and speciation in the field. However, experimental verification of reaction mechanisms and rate constants is needed to test the reliability of model predictions, particularly over the wide range of meteorological and environmental conditions likely to be encountered during pollution detection efforts. For many candidate signature compounds, data on chemical reaction pathways, decay product identification, and rates of decay or evolution in the near field are lacking. To fulfill these verification and parameterization gaps, real-time chemical characterization under natural yet reproducible environmental conditions is needed.

PNNL has successfully characterized the near field fate of pesticides, obscurants and other compounds using the wind tunnel at the PNNL Aerosol Research Facility. Data from these tests compare favorably with field measurements under similar conditions (e.g. Cataldo *et al*. 1989 and NRC, 1987). The environmentally controlled wind tunnel can simulate conditions that encompass arid to tropical conditions strictly controlled as to the specific humidity, temperature and sunlight regimes. It can provide background atmospheres containing contaminants typical of urban, agricultural, building or battlefield scenarios. The facility was designed with special back up power systems and chemical containment capabilities to enable the safe application of toxic and hazardous materials within the laboratory and wind tunnel. It is typically operated at negative air pressure to contain airborne materials and all effluent exhausted from the wind tunnel. The exhaust is passed through scrubbers and High Efficiency Particulate Air (HEPA) filters prior to release.

Real-time Fourier Transform Infrared (FTIR) spectroscopy and near-real-time gas chromatography (GC) are used to elucidate the chemistry under various test scenarios. To augment identification of the transformation products, mass spectrometry is used in conjunction with GC. This allows us to evaluate a remote sensing technology and confirm its results with a classic laboratory technique. When evaluating the near-field fate of a compound, the composition of the polluted air is analyzed in real-time to determine the stability of the chemical over 30 minutes or the length of time it would take a plume to travel up to 1500 m downwind at a wind speed of 0.9 m/sec (2 mph).

[1] PNNL is located on the U.S. Department of Energy's (DOE) Hanford Site in southeastern Washington.

For this study, four chemicals, pinacolyl alcohol (3,3-dimethyl-2-butanol), methyl iodide, methylphosphonic dichloride (dichloro-methyl-phosphine, DCMP), and thionyl chloride ($SOCl_2$), were identified as chemicals of interest for near-field fate assessments. Their molecular structures are shown in Figure 1.1.

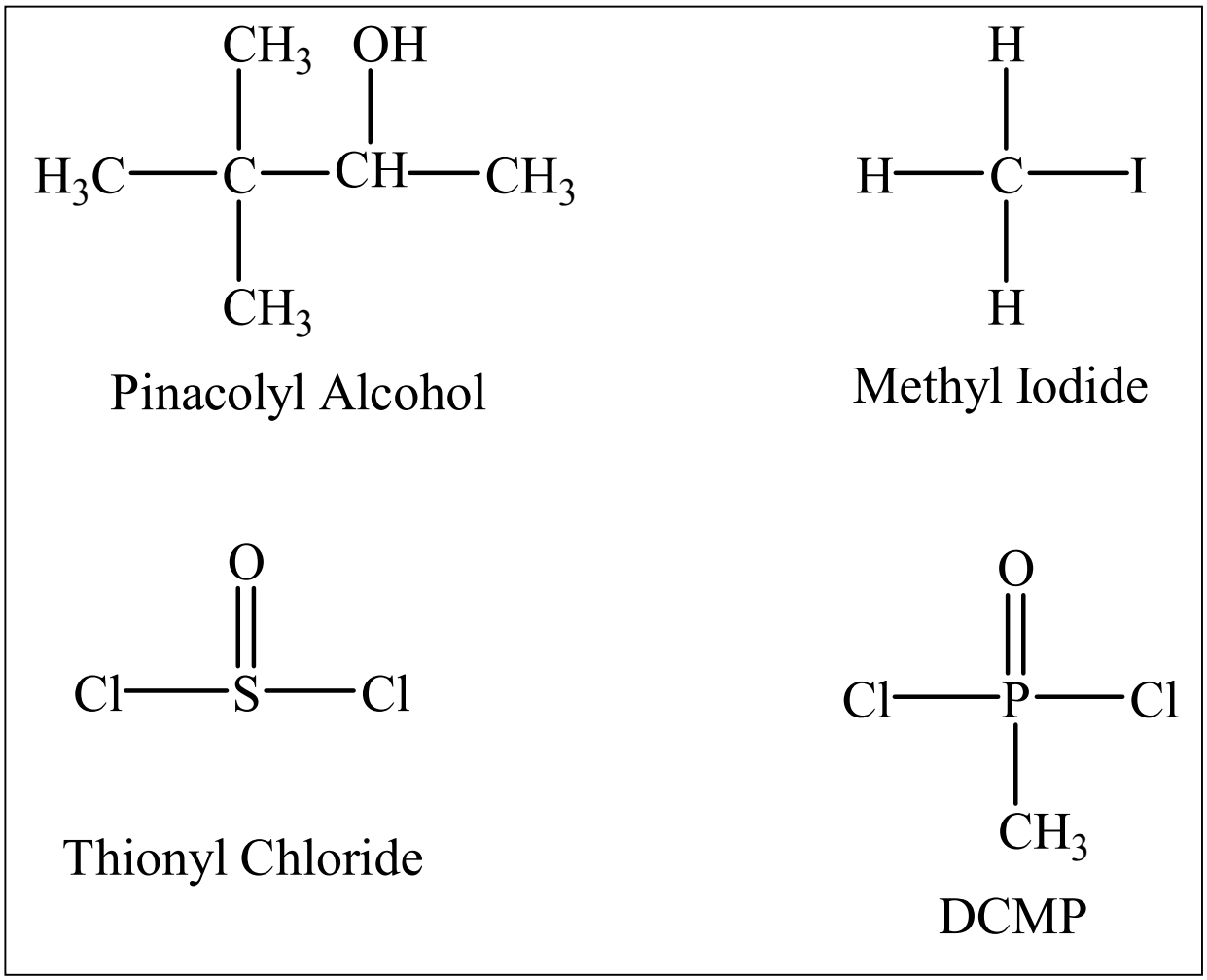

Figure 1.1. Chemical structures of the molecules studied in this report.

Fate data from these wind tunnel tests can be used to validate model output, provide empirical parameterization where data are lacking, and aid in reconciling field observations with model predictions, thereby enhancing the reliability and applicability of these assessment tools. In addition, data from these tests will also provide information on the suitability of specific chemical signatures for source identification and monitoring.

2.0 Experimental Approach

Each of the four chemicals was selected for testing because of its specific properties. Pinacolyl alcohol was selected because of its non-corrosive nature, low toxicity and non-reactivity. It was anticipated that this chemical would serve as a negative control for the system. As a compound known to photodissociate in the atmosphere (Roehl *et al*. 1997), CH_3I was used as a positive control. Methylphosphonic dichloride (or dichloro-methyl-phosphine, DCMP) was an example of a highly toxic phosphorous compound. Thionyl chloride ($SOCl_2$) was a representative highly reactive species, as it is known to hydrolyze in condensed phases.

The loss rate of the parent chemical and rate of evolution of any transformation products were monitored over a range of selected environmental conditions. The range of humidity and temperature into which the compounds were emitted simulated arid, temperate and tropical location values. Lighting regimes were used to simulate daytime, nighttime and conditions representative of the upper troposphere/lower stratosphere.

Rates of parent compound loss and evolution of transformation products under the various environmental conditions were monitored in real time. Two methods of continuous analysis were used: a GC equipped with automated gas-phase sampling, as well as time-resolved FTIR spectroscopy. Both techniques were employed to monitor chemical load in the wind tunnel during generation, test, and purge cycles. FTIR spectroscopy was selected because it is a broadband technique capable of detecting most molecular species with reasonably high sensitivity. Additionally, the FTIR spectroscopy configuration used here provides an effective simulation of EPA-aproved remote detection technology. Simultaneous analysis of the wind tunnel air by GC provided confirmation of the FTIR-determined mixing ratios and the relative sensitivity of this remote sensing technique. The combination of both methods also aids in identifying and evaluating the impact of interferences on remote and classical detection technologies. Mass spectrometry of periodic grab samples was also used to detect and/or identify transformation products over near-field transport time.

2.1 Wind Tunnel Test Configurations: Open-Loop / Semi-Dynamic Chamber (SDC)

The 70 m^3 environmental wind tunnel (Figure 2.1) located within the Aerosol Research Facility is constructed of stainless steel, except for the clear Lexan®[2] walls and portions of the ceiling of the primary test section. The remainder of the test section ceiling is constructed of quartz to allow passage of ultraviolet light from the stratosphere-simulation lighting. Wind speed, temperature, humidity, and lighting are controlled within the system to provide natural environments for testing. Most laboratory instrumentation is connected to a computer data acquisition system to control test parameters and for subsequent data analysis. The wind tunnel is typically operated in a continuous loop mode.

Most of the measurements were performed in the primary test section of the wind tunnel. This test section is 6.1 m long and 0.6 x 0.6 m wide (Figure 2.1). The inlet to the test section is shaped to provide uniform air flow with minimal wall turbulence; velocities are uniform within 3% over the width of the test section.

[2] Lexan is a registered trademark of the General Electric Company.

Water vapor was added to the system when higher humidity was required while dry synthetic air was introduced into the tunnel to lower the relative humidity below ambient. The humidity of the test atmosphere was typically measured during each test using a hygrocomputer[3]. A precision controlled draft sling psychrometer[4] was used as a secondary standard to confirm hygro-thermometer measurements periodically when the system was clean.

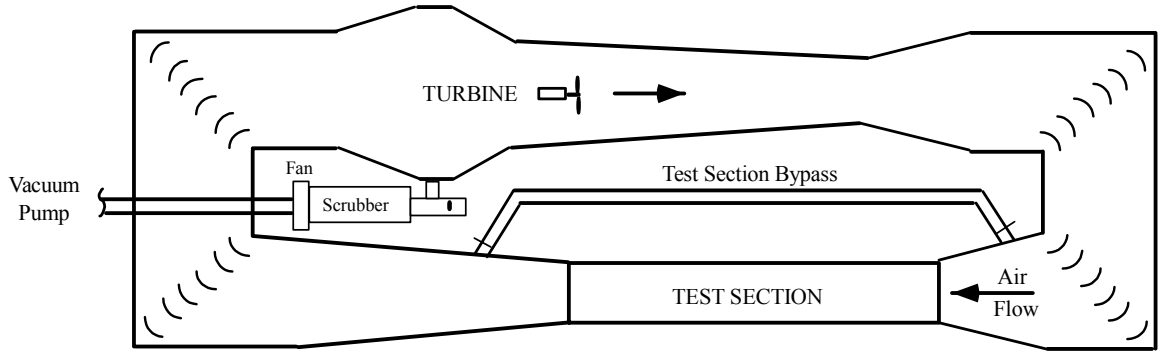

Figure 2.1. The PNNL wind tunnel (top view).

During the tests with methyl iodide, it was determined that the effective exposure time of the chemical to simulated sunlight was less than necessary to simulate near-field transport. To lengthen the exposure time to simulated sunlight and to minimize the exposure to corrosive chemicals, some of the CH_3I tests and all the DCMP and $SOCl_2$ experiments were performed in the SDC shown in Figure 2.2. This modified chamber occupied approximately 40% of the length of the original wind tunnel test section. Because of the large size of this chamber (and the resulting increased volume to surface-area ratio) the importance of any wall reactions was reduced. In addition, the inner wall, end plates, floor, and portions of the ceiling of this SDC system were lined and sealed with Teflon®[5] film to reduce chemical adsorption and any heterogeneous chemistry that may occur on the surface. Quartz windows, placed in the ceiling of 60% of the SDC (a total of 0.78 m^2), were left uncovered to prevent interference to UV light entering the chamber. The chamber was initially "conditioned" by introducing the test chemical into the SDC and allowing it to reside within the chamber for ~10 minutes prior to testing. The entire volume (800 L) was then purged and filled with room air adjusted to the desired temperature and humidity.

Samples for gas chromatographic (GC) analysis and/or gas chromatographic/mass spectrometry (GC/MS) analysis were withdrawn through ports inserted in window number 3 of the SDC. As shown in Figure 2.2, test chemicals were also introduced into the chamber through a separate port also located in window number 3.

[3] Model 5000, General Eastern Instrument Company, Wilmington Massachusetts.
[4] Assmann Psychrometer, Model 5230, All Weather, Inc., Sacramento, California.
[5] Teflon is a registered trademark of the E.I. du Pont de Nemours and Company and company or its affiliates.

Wind Tunnel Test Section (Shown the First 4 of 8 Windows)

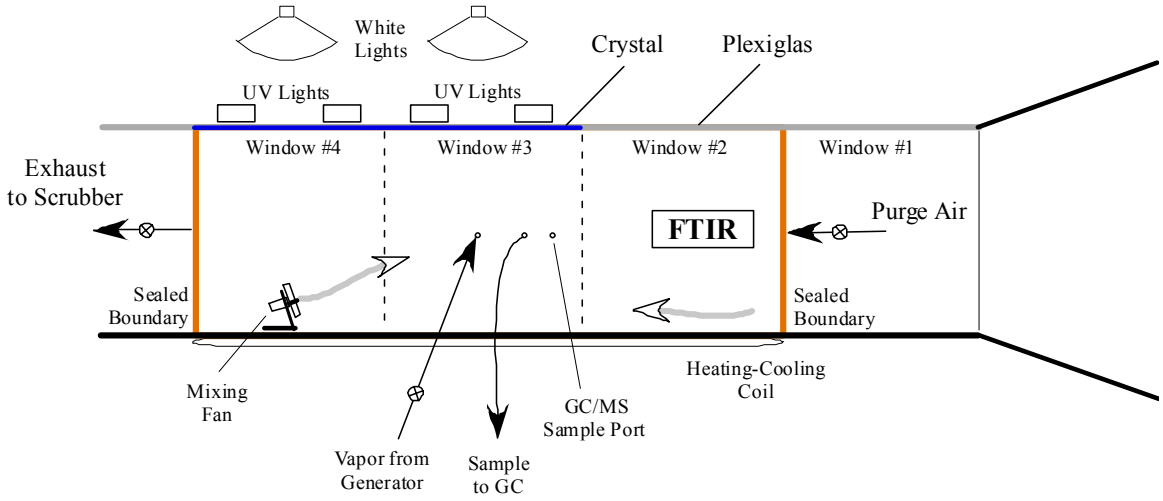

Figure 2.2. Semi-Dynamic Chamber (SDC). The SDC was used for studies requiring increased exposure time to simulated sunlight (side view showing the first 4 of 8 access windows).

The air in the SDC was continuously mixed with a fan during testing. This promoted a homogenous atmosphere within the system. Temperature was controlled through a heating-cooling water circulation system in the floor of the test chamber. The temperature and humidity of the SDC atmosphere were measured using a digital hygro-thermometer[6]. Lighting was provided by two 400 W metal halide lamps (ANSI M59) supplemented with 8 Sylvania 350 nm Black Light F20T12/350BLR 20 W lamps. Additional UV light was added during the methyl iodide photolysis tests to characterize its breakdown under wavelengths near its absorbance maximum (260 nm) with the addition of two 254 nm shortwave UV lamps[7]. Tests with lights on and lights off were performed for all test chemicals. The UV intensity near the centerline of the test system was measured with a broad-band UV meter[8] and was found to be ~50% of sunlight from the noon sun outside the laboratory (latitude 46° 30') near the autumnal equinox.

2.2 Analyses of Chemical Composition of Test Atmospheres

As discussed above, we used two independent means of measuring the change in concentration of vapors as a function of environmental parameters (FTIR and GC). Two independent methods were also used to identify chemical compounds (FTIR and GC/MS).

2.2.1 Fourier Transform Infrared (FTIR) Spectroscopy Analysis

The MIDAC FTIR was configured in a special optical arrangement to accommodate the layout of the PNNL wind tunnel and SDC. By placing an infrared source on one side of the wind tunnel and the detection FTIR on the opposite side, the wind tunnel effectively served as a spectrometer "sample compartment". The FTIR was able to serve both as a real-time monitor of the parent compound and as a means of identification of the decay products. The FTIR detection configuration is depicted in Figure 2.3. As shown in Figure 2.3, the Lexan® windows on both

[6] Omega Model 411 Digital Hydro-Thermometer Omega Engineering, Stamford Connecticut
[7] Model XX-15F SpectroLine Corp, Westbury New York
[8] UVM UV Meter, Apogee Instruments Inc., Auburn California

sides of section 2 contained 5 cm diameter zinc selenide windows, also uncovered, to permit cross-chamber transit of light from an infrared source[9] to the emission FTIR[10].

The source was a SiC Globar powered by a constant 12 V DC supply. Infrared light from the source was collimated using a 6-in. (15 cm) effective focal length 90°-off-axis paraboloid mirror. The collimated beam was transmitted through the tunnel using 5 cm antireflective-coated zinc selenide windows that provided both IR transmissivity and chemical durability. The source optics were configured with translation stages to optimize throughput and ease adjustment. The path through the wind tunnel was measured to be 24-3/8 inch (619.1 mm). Gases were well mixed and exhibited near-laminar flow (for flow experiments) in the region of the wind tunnel through which the infrared beam path passed.

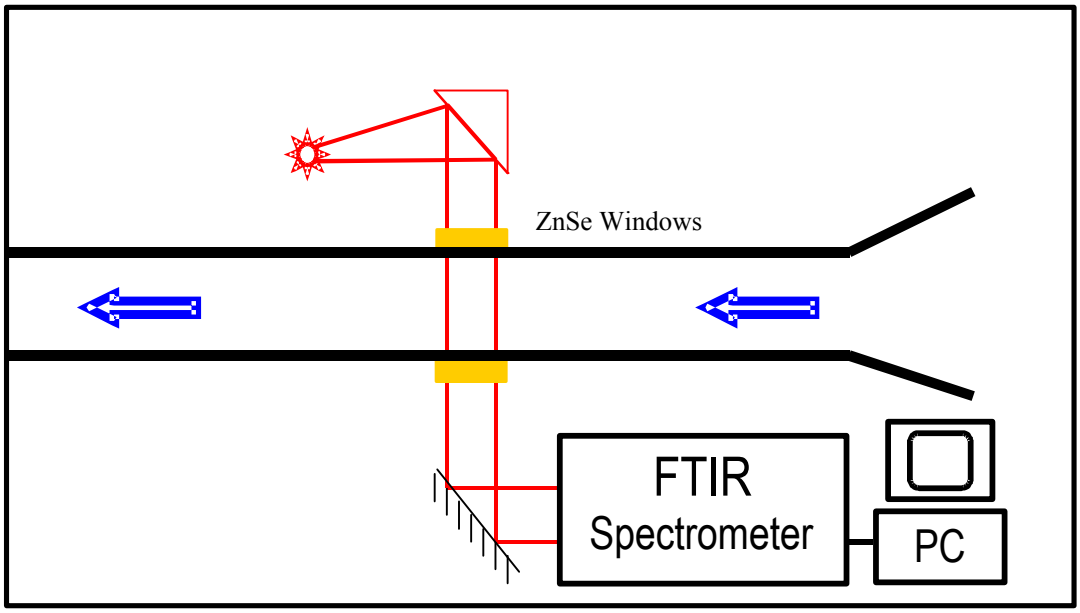

Figure 2.3. Schematic of optical layout of the FTIR spectrometer in the wind tunnel (top view).

On the detection side of the wind tunnel "sample compartment", the collimated beam was reflected into the MIDAC FTIR with an adjustment mirror. The light was coupled into the spectrometer through a zinc selenide window and modulated by an interferometer using a germanium/zinc selenide beamsplitter. The linear voice-coil interferometer modulated the IR light and the beam was focused onto a 77 K Infrared Associates[11] 16-0.5µm mercury cadmium telluride detector (0.5 x 0.5 mm). A specially configured 2.5µm long-pass filter (3900 cm^{-1} cut-on) was used to reduce the intensity on the detector and thus provide a more linear response. [The spectrometer was thus set for 4 cm^{-1} resolution for studies where the species of interest had infrared band half-widths ≥ 15 cm^{-1}.] The Fourier transforms were carried out (using triangular apodization, Mertz phase correction and 4x zerofilling) only at the end of each experiment to facilitate faster data acquisition. For other studies the resolution was increased as appropriate. The software for spectrometer control and data evaluation was MIDAC Grams32 Vers. 4.11[12] along with Wavemetrics' IGOR Pro

[9] SiC Globar, Niagara Falls New York purchased through MIDAC
[10] MIDAC Model M2401-C, MIDAC Corporation, Irvine California
[11] InfraRed Associates, Stuart Florida
[12] MIDAC Corporation, Irvine California

software, version 4.0.2.1[13]. Data are presented directly in absorbance mode, $A = -\log_{10} (I/ I_o)$, where the I_o reference spectrum was recorded just prior to each spectrum, or series of spectra. Time evolution data are presented as either 3D stacks (intensity vs. wavenumber vs. time) or as contour plots to aid in visualization.

Concentrations of various analytes were calculated from the FTIR studies according to the Beer-Lambert law of absorption:

$$A = \varepsilon C l \qquad (2.1)$$

where A = absorbance (log base 10)
ε = molecular absorption coefficient $(ppmV\text{-}m)^{-1}$
C = mixing ratio by volume (ppmV)
l = path length of the light through the sample in meters

Concentrations were derived by first using the reference spectrum to calculate an integrated band absorption coefficient and then applying this to the measured spectra. Although integrating over an entire band does make the calculation more susceptible to interferences from other species, the effects of noise and baseline drift are reduced (Griffith, 1996). In future experiments we intend to increase the sensitivity by folding the light path and thus achieving a greater absorbance signal without significantly increasing the noise.

Reference spectra were taken from the PNNL spectral database (Sharpe 2000, Sharpe *et al*. 2001, Johnson *et al*., 2002). In this database, each reference spectrum is reported as a fit to Beer's law constructed from 10 or more individual measurements at different burdens. The fit is constructed to represent exactly 1 ppmV-m at 25° C. The noise level is $< 5 \times 10^{-3}$ absorbance (root-mean-square) and the systematic error in intensity is < 3% (2σ).

2.2.2 Gas Chromatographic (GC) Analysis

Two separate gas chromatograph instruments were used. The first, used to monitor the concentrations of test chemicals, was an HP 5890 GC[14] equipped with an electron capture detector (ECD) and a flame ionization detector (FID). The GC was connected directly to the tunnel through 1/16 in (1.6 mm) Teflon® tubing via a custom-built gas-sampling manifold. Automated gas-phase sampling and analysis were made possible by in-house modifications to the GC, which included addition of a 6-port sampling valve and 12-port stream select valve[15] mounted in a temperature controlled valve oven along with necessary electronics, pneumatics, and plumbing to drive the valves. The injector, consisting of the 6-port pneumatically actuated sampling valve, was connected to a 1.0 ml sample loop. Gas was drawn continuously through the selected port at 50 ml/min using vacuum. The sample valve was maintained in the load position between chromatographic runs, then rotated into the inject position to introduce the contents of the sample loop directly onto the column at the beginning of the run. Either the ECD or FID were connected to the column outlet as appropriate for the compound to be detected. Data were processed through an HP Model 3396 integrator.

The elution time was typically varied for each chemical. For DCMP and $SOCl_2$, the GC was run at a constant temperature configuration, which ensured that the test chemical peak eluted at about 2

[13] Wavemetrics, Inc., Lake Oswego, Oregon
[14] Model 5890 Series II, Hewlett Packard, Palo Alto, California
[15] Valco, Houston, Texas

minutes. The total time for each chromatogram was 3 minutes resulting in a 3.5 minute cycle that included sample acquisition and dead time. GC measurements corresponded in real time to measurements made with the FTIR so that the temperature, humidity, and other parameters were identical.

The second GC, used to identify potential breakdown products in the wind tunnel, was a HP 5890 I GC connected to an HP 5970 mass spectrometer.[16] A GC/MS analysis was performed when concentrations decreased and transformation products were observed by FTIR or GC analysis. Samples were drawn by gas syringe from the wind tunnel and injected manually into the GC/MS at selected intervals during the experiment. The GC/MS instrument was calibrated with pure solutions of the test chemical at concentrations ranging from 1 to 100 ppm by weight. Where possible, mass spectra were compared to mass spectra in the National Institute of Standards and Technology (NIST) library and supplemented with the PNNL library of pesticide type compounds.

[16] Hewlett Packard Instruments, Palo Alto California

3.0 Pinacolyl Alcohol Experiments

A total of 20 experiments evaluated the effect of the following environmental variables on near-field fate of pinacolyl alcohol (PA): relative humidity (RH) of 30%, 40% 50%, and 80%, temperatures of 25°C and 35°C, and simulated sunlight. Typically, three replicate tests were performed for each environmental variable. PA was introduced into the wind tunnel until its concentration reached 80 to 100 ppmV. Concentration data were collected during the subsequent near-field transport simulation (25 to 30 minutes) and the loss rate of the alcohol during this period was calculated from a plot of the pinacolyl alcohol-mixing ratio (ppmV) vs. time (seconds).

3.1 Chemical Vapor Generation

The vapor generation system for pinacolyl alcohol[17] is shown in Figure 3.1. A chemical metering pump[18] delivered PA liquid onto glass beads in a glass column. Heated nitrogen (~65°C) flowed through the column and carried the vapor out of the generator to the wind tunnel. The flow rate of nitrogen was adjusted to ensure all the liquid in the glass column was vaporized. Concentration of the chemical in the wind tunnel was controlled by adjusting the delivery rate of the chemical metering pump. The whole generation system was enclosed in a vented fume hood.

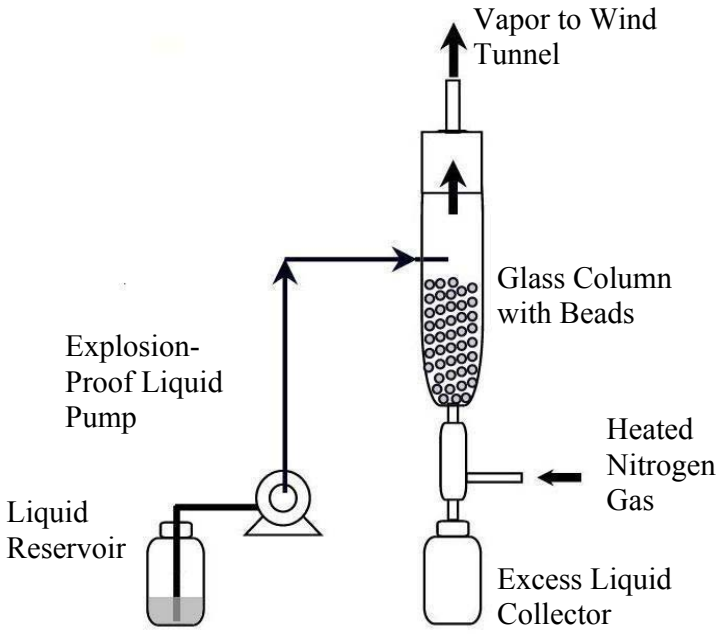

Figure 3.1. Pinacolyl alcohol vapor generation system.

[17] Aldrich Chemical, Milwaukee, Wisconsin. 98% purity, CAS # 464-07-3 (3,3-dimethyl-2-butanol)
[18] Model QDX explosion-proof pump, Fluid Metering, Inc., Syosset, New York

3.2 Gas Chromatograph Analysis

The HP 5890 II GC, equipped with a FID was used to analyze gas phase samples as described in section 2.2.2. A 15 m x 0.53 mm (i.d.) DB-Wax micro bore column with a 1 µm film thickness[19] was used for chromatography of pinacolyl alcohol in the gas phase. The GC oven was maintained at 50°C for two minutes and nitrogen was utilized as the carrier gas with the electronic pressure control set at 6.0 psi. Injection valves were heated to 200°C and the FID was maintained at 230°C.

Calibration of this GC system was accomplished using Tedlar gas-sampling bags[20]. Calibration standards containing 390, 130, and 32.5 ppmV were prepared by spiking 6, 2, and 0.5 µL of the test chemical directly into the Tedlar gas bags and then diluting the vapor with 3 L of room air. A fourth standard (3.25 ppmV) was prepared by diluting 0.3 L of the 32.5 ppmV standard with 2.7 L of room air. Triplicate samples were collected from gas bags through the 3 ports used during the test series for each of the four concentrations (total of 9 samples per concentration). Figure 3.2 shows the area units recorded for each concentration of the gas for all ports of the online GC vapor sampler. A linear equation was derived from the concentration vs. response data and this equation was subsequently applied toward measurement of unknown samples. Changes in the gas phase concentrations of pinacolyl alcohol during the test series were followed by automated injection of 1.0 ml samples of the wind tunnel atmosphere into the GC at two-minute intervals.

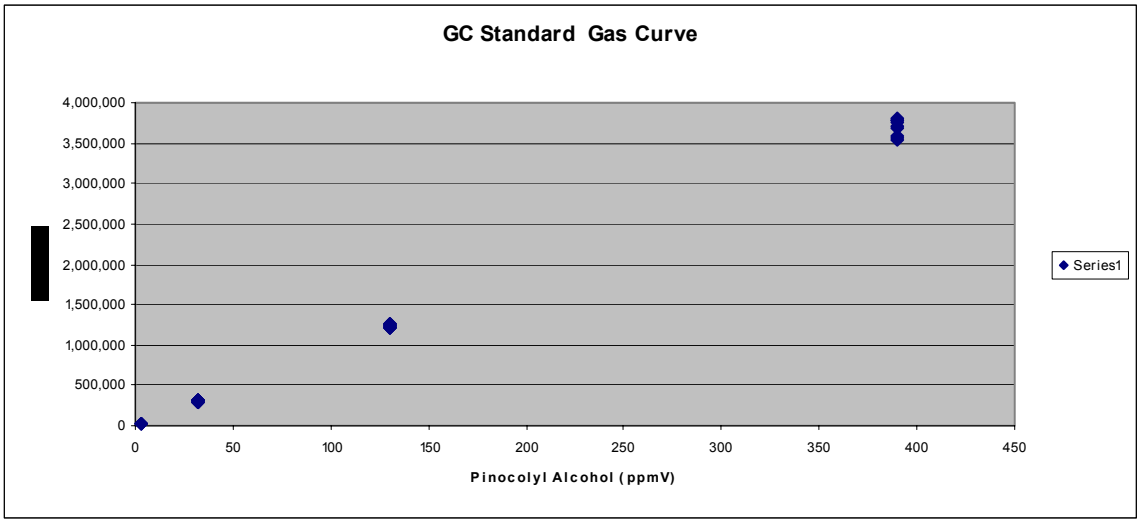

Figure 3.2. Pinacolyl alcohol calibration curve for the online GC vapor monitor. ($y = 9464.2x + 3487.5$; $R^2 = 0.9987$)

3.3 FTIR Analysis

As seen in Figure 3.3, pinacolyl alcohol has significant IR structure in the atmospheric window between 700 and 1300 cm^{-1}. Its strongest band, however, arises due to the C-H stretching motion is in an atmospheric window in the mid-wave IR near 2900 cm^{-1}. This band was used for PA

[19] J&W Scientific, Folsom California
[20] Supelco, Bellefonte, Pennsylvania

detection in these studies. The IR reference spectrum of the PA was recorded as part of the PNNL DOE IR database (Sharpe, 2000). The reference spectrum displayed in Figure 3.3 represents a composite spectrum normalized to 1 ppmV-m from a weighted average of more than 10 individual spectra, each recorded at a different burden.

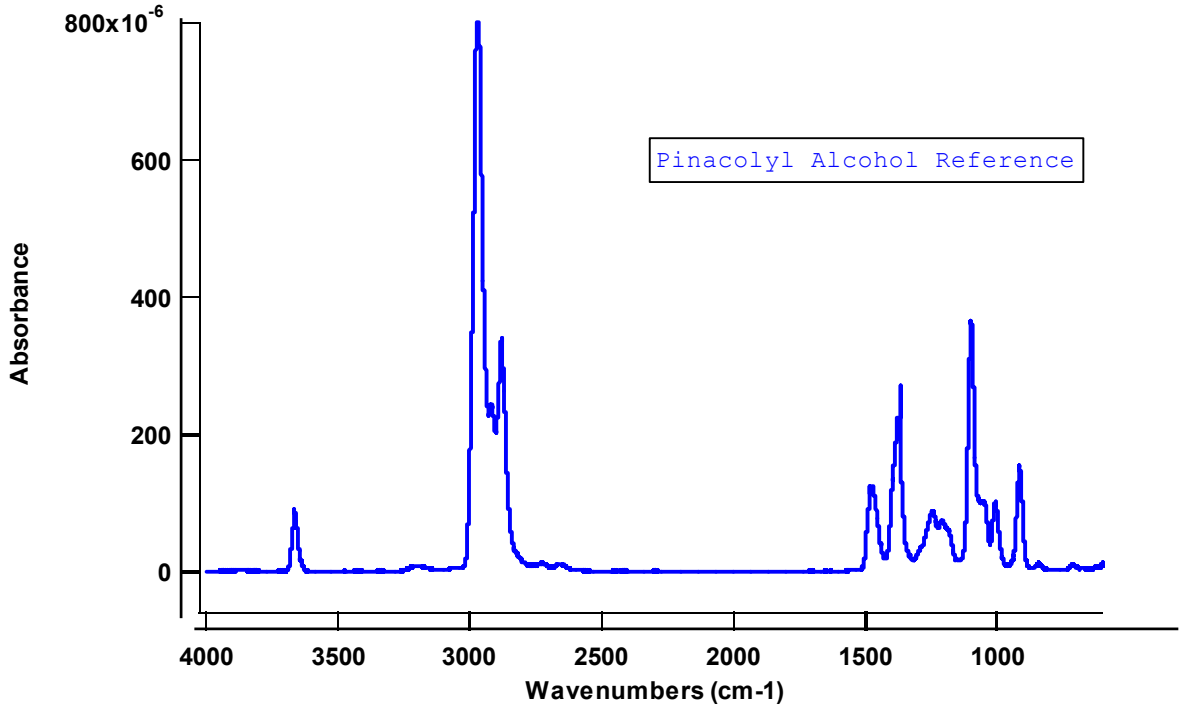

Figure 3.3. Reference IR spectrum of pinacolyl alcohol. Spectral resolution is 0.1 cm^{-1} and the absorbance values represent a burden of 1.0 ppmV-m.

The spectral resolution was set to 8 cm^{-1} because of the relatively broad nature of the C-H absorption band (width > 50 cm^{-1}). The concentration of PA was monitored directly from the absorption values and the data reduced by baseline correcting the individual spectra using a multiple point fit. Individual absorbance values were then extracted by integrating the C-H band.

3.4 Results

The raw absorption spectra for a typical concentration growth curve obtained by FTIR are presented in Figure 3.4. An absorbance contour plot of the C-H region for the same data is shown in Figure 3.5. Upon integrating the C-H band shown in Figures 3.4 and 3.5 and calculating the actual mixing ratio (in ppmV) from the individual spectra, the resulting growth and depletion curves are presented in Figure 3.6. The concentration data in this figure show a linear increase over the first ~30 minutes (generation of PA into the tunnel) followed by a slow linear decrease for about 20 minutes following cessation of the generation. The remaining data reflect the purge phase. Loss curves were also obtained by near-real time analysis of the wind tunnel air by GC (Figure 3.7) and were similar to those obtained by FTIR spectroscopy.

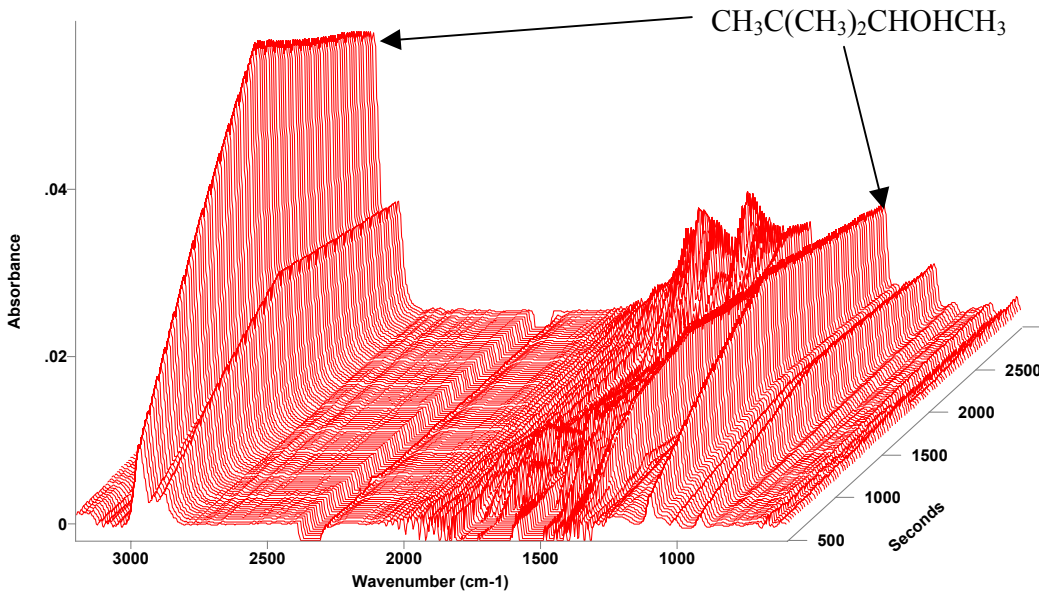

Figure 3.4. Three-dimensional stacked dynamic infrared spectra of pinacolyl alcohol. The relative humidity was 80%, the spectral resolution was 8 cm^{-1} and the acquisition time for an individual spectrum (i.e. time between files) is 25.5 seconds.

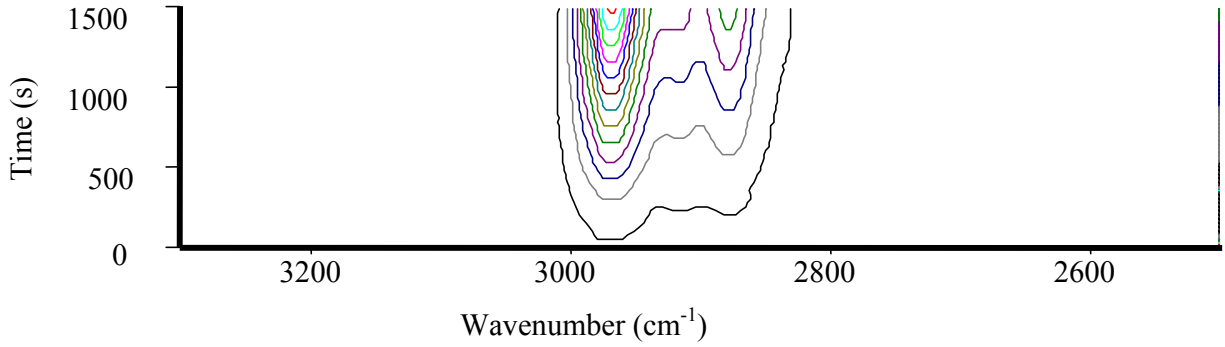

Figure 3.5. Absorbance contour plot of the C-H region for pinacolyl alcohol during the 80% RH study test. The spectral resolution was 8 cm^{-1} and the acquisition time for averaged spectra (i.e. time between files) is 25.5 seconds.

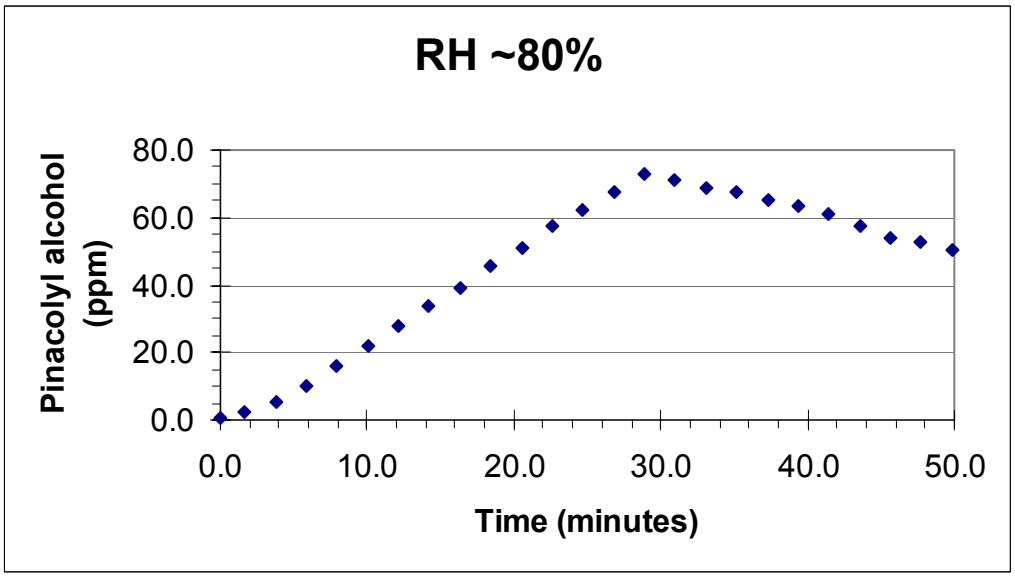

Figure 3.6. Typical generation and loss curve of pinacolyl alcohol obtained by FTIR. In this test the alcohol was generated into an atmosphere of 84% RH and 26°C. Four spectra were averaged to generate a data point representing approximately 2 minutes. The alcohol loss rate is -9.9×10^{-5} sec.

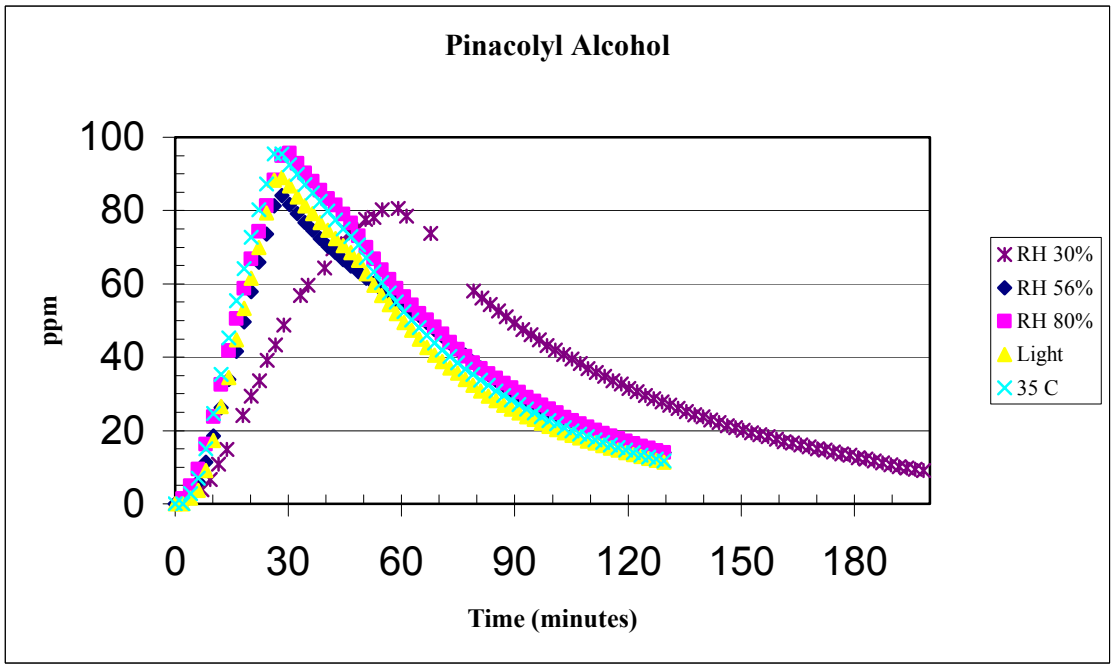

Figure 3.7. Generation and loss curves of pinacolyl alcohol as determined by gas chromatography under varying humidity and lighting regimes. Note that the loss curve under the 30% RH test conditions depicts a slower sample introduction rate and a prolonged loss phase without a subsequent purge phase.

3.5 Data Analysis

The experimentally observed loss rate of PA was modeled as follows:

$$\frac{d[PA]}{dt} = -k_{dil}[PA] - k_{decay}[PA] \quad (3.1)$$

where k_{dil} is the first-order dilution loss rate coefficient and k_{decay} is the first-order loss rate coefficient of the other removal processes (hydrolysis, photolysis, wall effects).

Therefore, loss due to dilution alone is

$$\tau = 1/k_{dil}\,[PA] = [PA]_o \exp(-k_{dil}\,t) \quad (3.2)$$

while the loss due to both processes is

$$\tau = 1/(k_{dil} + k_{decay})\,[PA] = [PA]_o \exp(-(k_{dil} + k_{decay})t) \quad (3.3)$$

where τ is the observed decay lifetime (sec) and $[PA]_o$ is the initial concentration of the alcohol.

An orifice plate was installed in the wind tunnel exhaust pipe to determine the airflow from the wind tunnel to the scrubber. With the exception of one test, the pressure drop across the orifice was 2 cm-water which indicated that the air flow rate was ~33 ft^3/min (cfm). The exception occurred during the second run of the 56% relative humidity tests when the pressure drop rose to 5 cm-water indicating a flow rate of ~50 cfm. Because of the pressure drop, uncontaminated room air was continuously drawn into the wind tunnel to maintain the air balance, and a slow dilution of PA concentration in the wind tunnel occurred during the course of each test. By extracting a constant volumetric airflow from the wind tunnel, the alcohol lost is proportional to its concentration, a first order loss process.

To compare the concentration profiles of PA under various environmental conditions, the loss rate at 30% RH and 25°C was used as a baseline. The alcohol loss rates determined for the remaining environmental conditions were compared to this baseline rate. The concentration profiles were also compared by expressing the concentration as a percentage of initial concentration (concentration at the beginning of decay) as a function of time. Analysis of covariance was used to determine whether the slopes of the loss curves were significantly different. A Newman-Kuels multiple range test was used to separate the slopes if the analysis of covariance concluded the slopes were not equal. Following the post-generation near-field simulation period, the wind tunnel air was purged with fresh air for 60 minutes or until an uncontaminated background was attained.

During the initial release and depletion phase of each experiment prior to scrubber operation a pressure differential of 6 mm of water (6×10^{-4} atm) was maintained between the inside and outside of the wind tunnel; slow dilution of the chemical thus occurred following the cessation of the generation phase. The calculated loss curve due to dilution is shown in Figure 3.8. The slope of this curve (the loss rate) is 1.014×10^{-4} s. To compare the concentration profiles of pinacolyl alcohol under the various meteorological conditions to the dilution loss rate, the observed concentrations of the alcohol were expressed as a percent of initial concentration (concentration at the beginning of decay) and plotted as a function of time post-generation (Figure 3.9).

The mean loss rates of pinacolyl alcohol under varying conditions of humidity, temperature and light conditions (listed in Table 3.1) show no evident difference from the predicted dilution rate. The minor differences observed are smaller than the experimental uncertainty of ~6% (based on the standard deviation of experiments). Therefore, the observed differences cannot be attributed to an environmental cause

Table 3.1. Concentration Decay Constants of Pinacolyl Alcohol Under Differing Environmental Conditions. (Values are mean ± one standard deviation.)

Humidity (%)	Temp (°C)	No. Tests	Loss Rate[a]	± 1 SD
Relative Humidity Experiments				
30	24.7	2	-0.000095	± 0.0000058
40	24.5	2	-0.000104	± 0.0000048
56	24.9	3	-0.000099	± 0.0000013
84	26.2	3	-0.000096	± 0.0000046
Temperature Experiment				
25	34.8	3	-0.000102	± 0.0000023
Sunlight Experiment				
50	25.3	3	-0.000102	± 0.0000011

[a] Loss rate (sec) determined from an exponential curve fit to the experimental data.

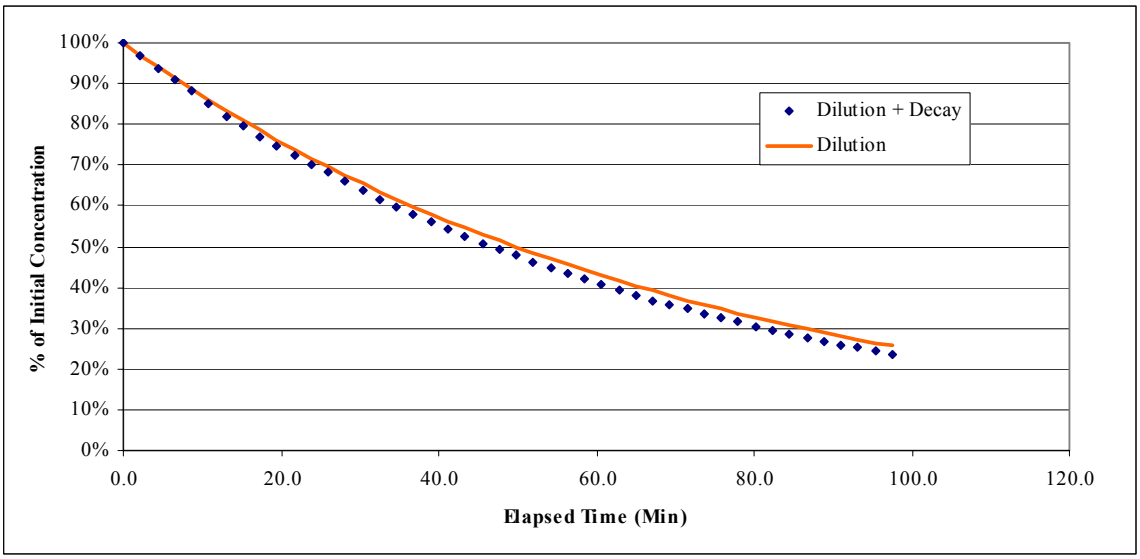

Figure 3.8. Calculated and measured loss of pinacolyl alcohol. The calculated loss (solid line) due to dilution of the plume from maintaining a negative pressure within the wind tunnel. The measured loss (dotted line) under baseline conditions of 30% RH and 25°C is also pictured.

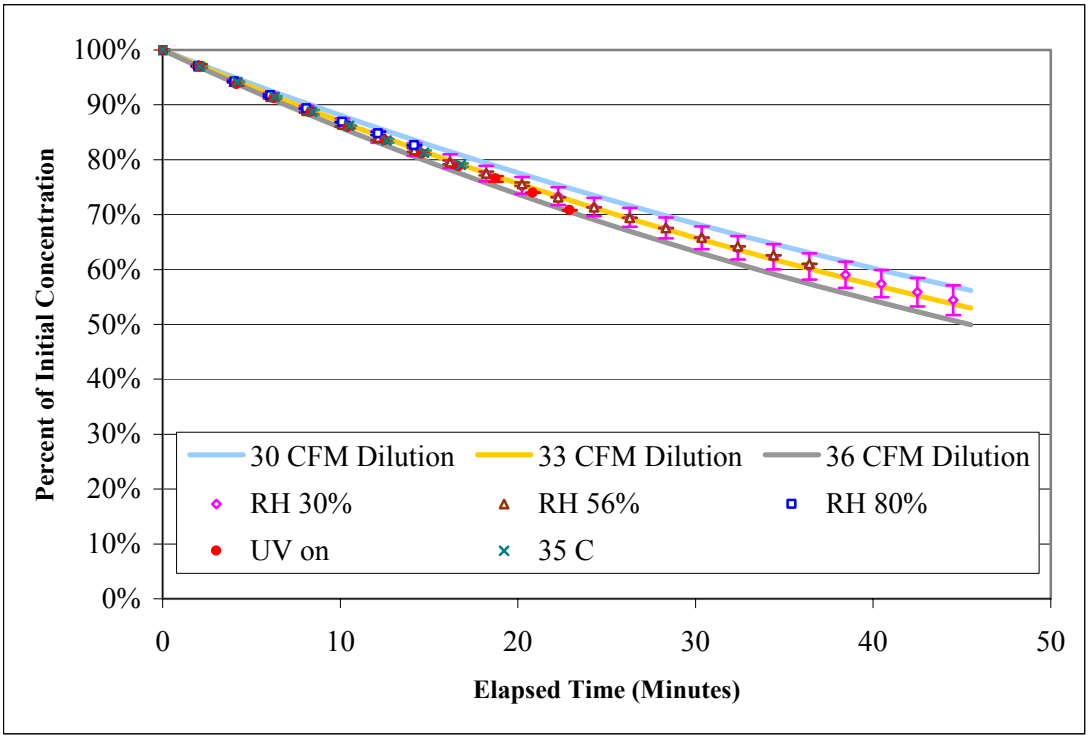

Figure 3.9. Loss of pinacolyl alcohol under various environmental conditions expressed as a percentage of the initial concentration. Symbols represent the average and the bars show the range of concentrations. The calculated loss due to dilution from maintaining a slightly negative pressure is also depicted as three solid lines on the figure (calculated using 30, 33 and 36 cfm dilution rates).

3.6 Potential Use of Vegetation Off-Gassing

Plants are important sinks for many airborne contaminants and are known to re-emit to the atmosphere many of the volatile organic compounds that have previously diffused into the leaf (sub stomatal cavities) through open leaf pores (stomata). This is particularly true when the surrounding air is depleted in the compound (e.g., shut-down of source term) (Bennett *et al*. 1973a,b; Riederer 1995; Welke *et al*. 1998).

To test the potential for using this non-invasive measurement of leaf emissions for emission history of PA, we conducted a preliminary test of the uptake and off-gassing of the alcohol in a mixture of temperate and tropical vegetation. A PA concentration of 12 to 14 ppmV was established in the entire wind tunnel. Once a stable concentration was reached, isolation barriers were raised to separate the test section from the rest of the tunnel. A by-pass duct was opened simultaneously to retain the airborne concentration in the rest of the wind tunnel. The test section was then purged with laboratory air until the alcohol could not be detected by gas chromatography. At this point the test section was opened and a variety of plant species introduced into about 0.6 m^2 of the test section (Figure 3.10). The soil and plant containers were covered with aluminum foil. The isolation barriers were then lowered and the by-pass closed. The PA concentration was re-established in the test section within about 6 minutes and maintained for 1 hour. A purge period of 2 h followed as the chemical was evacuated from the test section, the plants were then removed to a clean atmosphere and the foil coverings removed from the pots (1 hour outside the tunnel). The plants were then placed into a lighted glove box and the pinacolyl alcohol concentration in the

glove box atmosphere monitored for about 40 minutes by gas chromatography (Figure 3.11). The volume of the glove box was 300 liters.

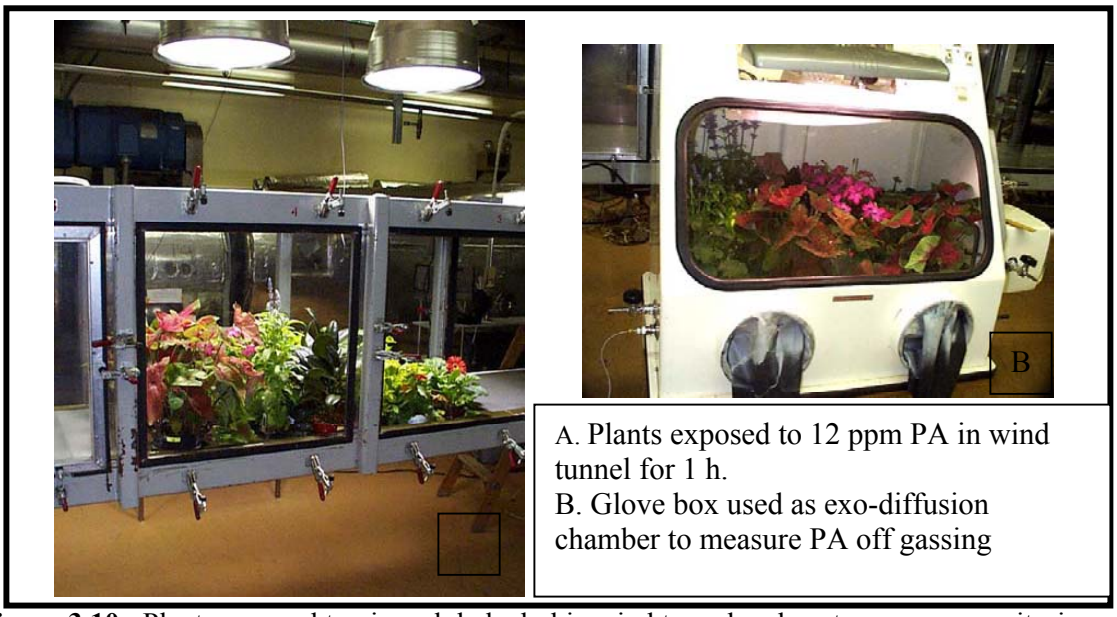

Figure 3.10. Plants exposed to pinacolyl alcohol in wind tunnel and post-exposure monitoring of plant emissions.

As shown in Figure 3.11, upon removing the vegetation to a clean system, PA emissions from the plants were monitored by gas chromatography for ~40 minutes, but several hours after exposure had ceased. As can be seen, the PA concentration due to off-gassing grows steadily, stabilizing near 1.6 ppm.

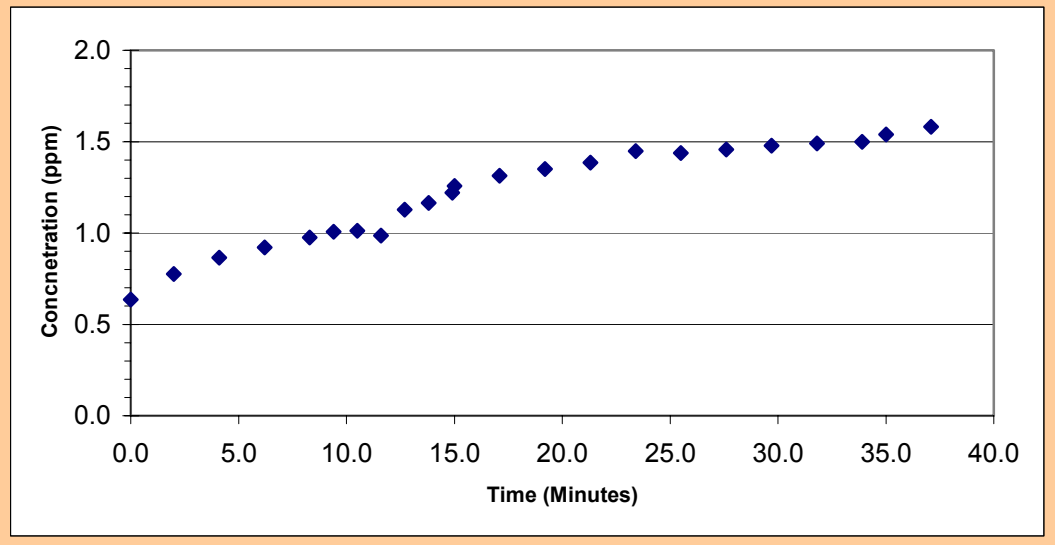

Figure 3.11. Emission of pinacolyl alcohol from exposed vegetation. These emissions occurred 3 hours after the plants were removed from the exposure system (wind tunnel) and placed in a clean atmosphere.

3.7 Discussion

FTIR and GC provided comparable detection sensitivity for PA under the various test atmospheres. The concentration data showed that the loss rate of the alcohol was negligible in near-field simulations and was insensitive to field relevant ranges of temperature and humidity. UV radiation simulating sunlight showed no effect on the short-term stability of the compound. However, the actual exposure of the chemical to simulated sunlight was minimal because of the relatively short residence time under the lighting system during the near-field simulations. Therefore, a semi-dynamic system that allows for more prolonged exposure to light was constructed to test the remaining chemicals.

The results of this study verify the stability and usefulness of pinacolyl alcohol as a signature in near-field scenarios under a wide range of meteorological conditions and demonstrated that wall effects and other interferences were minimal within the dynamic test system. No direct measurements of rate coefficients for this species, nor any structure activity relationships (SAR's) for similar alcohols were found in the literature. Because this alcohol is only minimally soluble in water and because it is thermally stable over the environmental range tested, only minor changes in atmospheric loss rate of pinacolyl alcohol due to temperature and humidity would be expected. While an hydroxyl reaction rate coefficient for this chemical is likely to lie between that of 2,2 dimethyl-propanol (5.5×10^{-12} cm^3/molecule-s) (Atkinson, 1994) or 1-butanol (8.6×10^{-12} cm^3/molecule-s), and 1-pentanol (1.1×10^{-11} cm^3/molecule-s) (Atkinson, 1994) it is most likely closesr to the latter. A reaction rate of 1.0×10^{-11} cm^3/molecule-s can be estimated with about ±20% uncertainty. This loss rate would not significantly affect concentrations in the near-field for daytime mid-latitude conditions.

In addition, the results show that gaseous diffusion of pinacolyl alcohol into leaf pores (stomata) occurs and that the equilibrium status of exposed leaves can be utilized for remote and non-invasive onsite detection of signature compounds for at least several hours post exposure. The leaf acts as a chemical storage medium and when the ambient concentration of the pollutant is reduced due to production shutdown (e.g., in anticipation of inspection), net diffusion is out of the leaf and the volatile or semi-volatile signature is available for detection in the local area.

4.0 Methyl Iodide Experiments

The chemical fate of methyl iodide (CH_3I) was monitored at 21°C under conditions of either low relative humidity (30%) or high RH (75%) in the continuous loop operation of the wind tunnel. A slight pressure differential between the inside and outside of the wind tunnel was maintained during these experiments resulting in a slow dilution of the chemical as described in Section 3.0. CH_3I was generated into the wind tunnel until concentrations of 8 to 10 ppmV were obtained, at which time the introduction of CH_3I was terminated and then the tunnel air was monitored until the CH_3I concentration reached about 3 ppmV (>50 minutes). Because it was found that concentration changes below about 4 ppmV were difficult to detect by FTIR, a change was made to the monitoring protocol and the tests re-run so that concentration data were collected for the first 25 minutes (to a CH_3I concentration of about 6 ppmV) as previously described. This was followed by a second sampling period of >20 minutes during which the pressure differential between the test section and the room atmosphere was brought to near zero. A total of 7 tests were conducted to determine the effect of humidity on CH_3I's fate.

Since CH_3I is known to photolyze (Waschewsky *et al*. 1996), four photolysis studies were also conducted in the semi-dynamic chamber previously described in Section 2.1. Figure 2.2 shows the configuration of the test system used for the photolysis tests. During these tests the simulated sunlight at the earth's surface (wavelengths > 290 nm) was augmented with UV light from mercury lamps[21] having an emission maximum at ~254 nm. The 254 nm maximum emission was to simulate the light fluxes of the upper troposphere and stratosphere. Fortuitously, the 254 nm emission matched well the absorption maximum (262 nm) of the CH_3I as reported by Roehl *et al*. (1997). To assure adequate detection by FTIR spectroscopy as well as gas chromatography, the starting concentrations for the photolysis experiments were above 35 ppmV. After CH_3I was introduced into the system, the delivery line was purged with ultra-high purity (UHP) nitrogen to ensure no CH_3I would enter the system during the loss phase of these tests. The baseline dilution rate in the semi-dynamic chamber was established during the first 20 minutes post-generation after which the sunlight exposure was initiated. The wind tunnel air was purged with fresh air for 60 minutes following each test run.

4.1 Chemical Vapor Generation

Because the vapor pressure of CH_3I is 410 mmHg at 20°C, a simple vapor generation assembly (Figure 4.1) was used to deliver CH_3I vapor to the wind tunnel. Approximately 10 ml of CH_3I were placed in a flask[22]. UHP nitrogen passed through the headspace of the flask and carried CH_3I vapor to the wind tunnel. The concentration of CH_3I in the wind tunnel was controlled by adjusting the nitrogen flow rate through the flask containing the neat chemical. Under continuous loop operation, the concentration of the methyl iodide reached about 10 ppmV. Because quantification of CH_3I depletion by FTIR proved difficult at this starting concentration, higher concentrations (about 35 ppmV and 100 ppmV) were introduced into the semi-dynamic system for subsequent photolysis studies.

[21] Spectroline Model XX-15F, Spectronics Corporation, Westbury, New York
[22] Sigma Chemicals, St. Louis, Missouri, lot results 99.9%, CAS #74-88-4

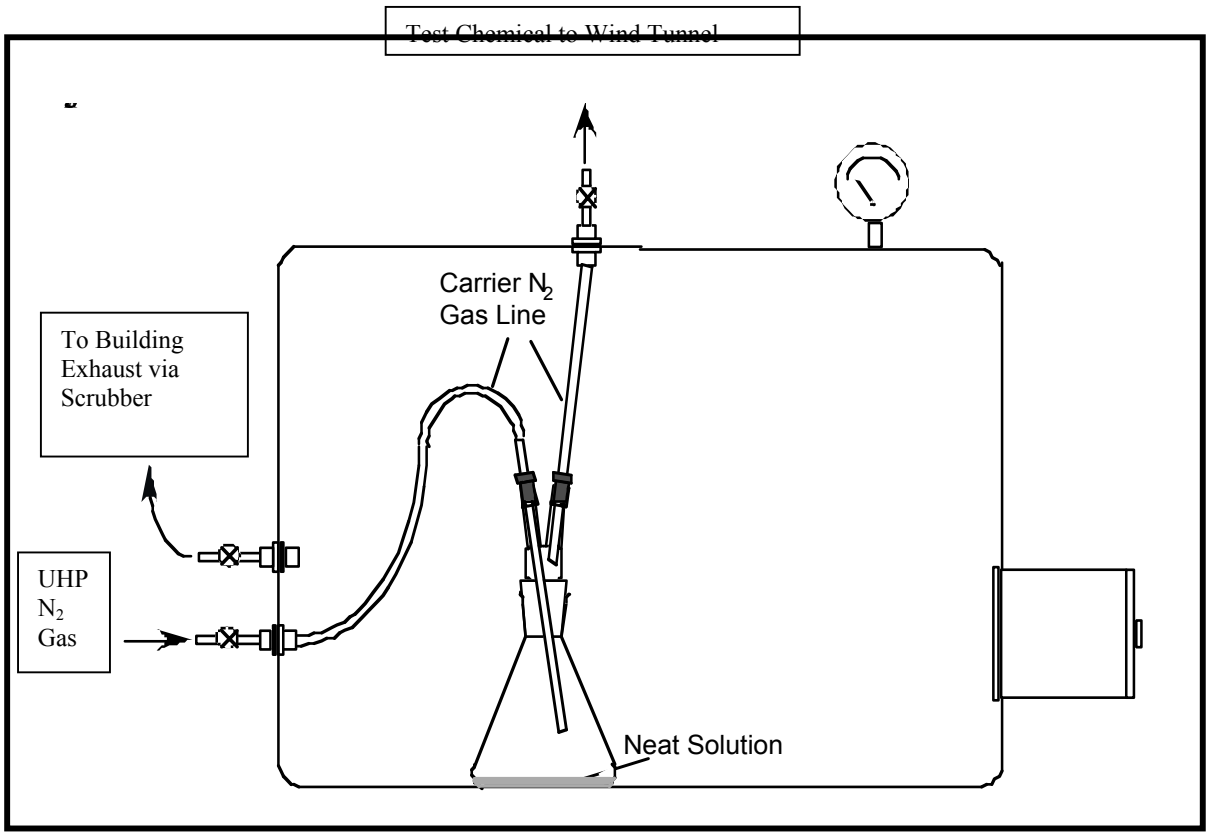

Figure 4.1. Methyl iodide vapor generation system.

4.2 Gas Chromatography Analysis

Changes in the gas phase concentration of CH_3I were monitored by automated injection of 1.0 ml samples of the wind tunnel atmosphere at 2.5-minute intervals into an HP 5980 II GC equipped with an ECD (Section 2.2.2). Gas phase samples were injected as described above onto a fused silica capillary column[23] (30 m x 0.53 mm i.d. 25m x 0.53 mm i.d.). The GC oven was held at 170°C for two minutes. N_2 was utilized as the carrier gas with the electronic pressure control set at 13.0 psi. The ECD was maintained at 300°C. For the detection of other iodinated compounds, the following oven temperature program was utilized: Hold at 110°C for 2 minutes, increase to 185°C at 25°C per minute, hold for 2 minutes.

Calibration of this GC system was accomplished using Tedlar gas-sampling bags[24] prepared from a certified 100 ppmV CH_3I gas[25]. The highest calibration standard was prepared by filling a Tedlar gas-sampling bag with 100 ppmV CH_3I. Concentrations of 10, 1, 0.1, and 0.01 ppmV were prepared by serial dilution from the 100 ppmV gas-sampling bag. An initial linear fit of the data above 25 ppmV proved unsatisfactory; therefore a quadratic equation was derived from the concentration vs. response data and applied toward measurement of unknown samples over the range from 0.01 to 100 ppmV.

[23] GS-Q fused silica capillary column, J&W Scientific, Folsom California
[24] Supelco, Bellefonte Pennsylvania
[25] Scott Specialty Gases, San Bernardino California

4.3 FTIR Analysis of Methyl Iodide

The IR reference spectrum for CH_3I was obtained from the PNNL DOE IR database (Sharpe, 2000). The reference spectrum displayed in Figure 4.2 is an average constructed from more than 10 individual spectra, each recorded at a different burden, all at 25°C. As seen, CH_3I has significant IR structure in the atmospheric window between 700 and 1300 cm^{-1}. Specifically, its strongest integrated band is near 1250 cm^{-1} in the long-wave infrared atmospheric window (Figure 4.2b). However, this band is directly adjacent to the absorption lines of the water ν_2 bending mode and some vapor phase water interference at high humidity fluctuation was observed. The MIDAC spectrometer did not have sufficient resolution to resolve individual rotational lines, but the strong Q-branch of this band could be resolved and aided in distinguishing the CH_3I from water. Although CH_3I could be identified using the 1250 cm^{-1} band, interference prevented quantification during tests where the atmospheric concentration was below 5 ppmV (open-loop humidity tests). For the wind tunnel studies with CH_3I, the spectral resolution was increased to 4 cm^{-1}. Prior to integration, the spectral bands were baseline corrected. The CH_3I concentrations were then derived by integrating the 1250 cm^{-1} band in the absorption spectra.

(a) (b)

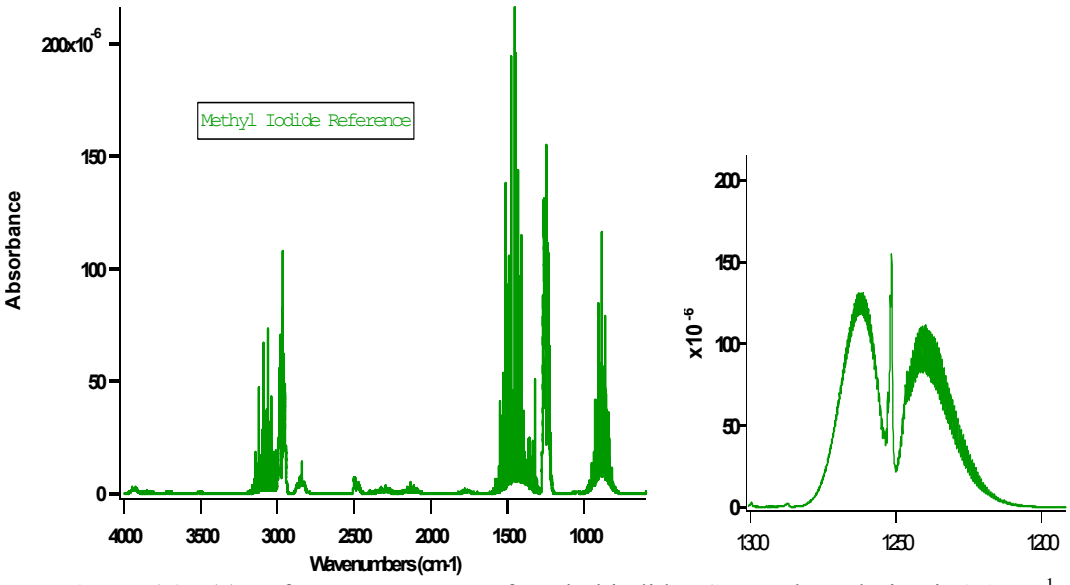

Figure 4.2. (a) Reference spectrum of methyl iodide. Spectral resolution is 0.1 cm^{-1} and the absorbance values represent an optical depth of 1.0 ppmV-m. At right (b), is an expanded view of the 1250 cm^{-1} band.

4.4 Results

During the humidity tests the target concentration of CH_3I during the generation phase was about 10 ppmV. While easily detected by GC (Figure 4.3), this concentration of CH_3I was insufficient for FTIR quantification under the water vapor conditions of the humidity tests. The IR absorption

cross-sections of CH_3I were not especially strong, and the signal was susceptible to interferences from the water lines (*vide supra*). The FTIR detection limit (signal: noise >3) for 1 minute averaging time during these tests was about 5 ppmV.

However, quantification of CH_3I at low concentrations was achievable by GC (Figure 4.3). As shown, the loss rate of the CH_3I was the same regardless of the humidity within the testing environment. Moreover, the loss rate observed in the humidity experiments did not differ from that of the loss rate due to the dilution of the chemical as a result of maintaining a pressure differential between the inside and outside of the wind tunnel (Figures 4.3 and 4.4). This is further corroborated in the non-diluted phase of the test (i.e., with pressure differential between the inside and outside of the wind tunnel near zero) when no significant loss of the iodide due to hydrolysis was observed (Figures 4.3, and 4.4). However, when UV exposure was applied to the 75% RH atmosphere, the CH_3I concentration appeared to decrease somewhat, but the loss rate was low (Figure 4.4) due to the short residence time under the UV lamps.

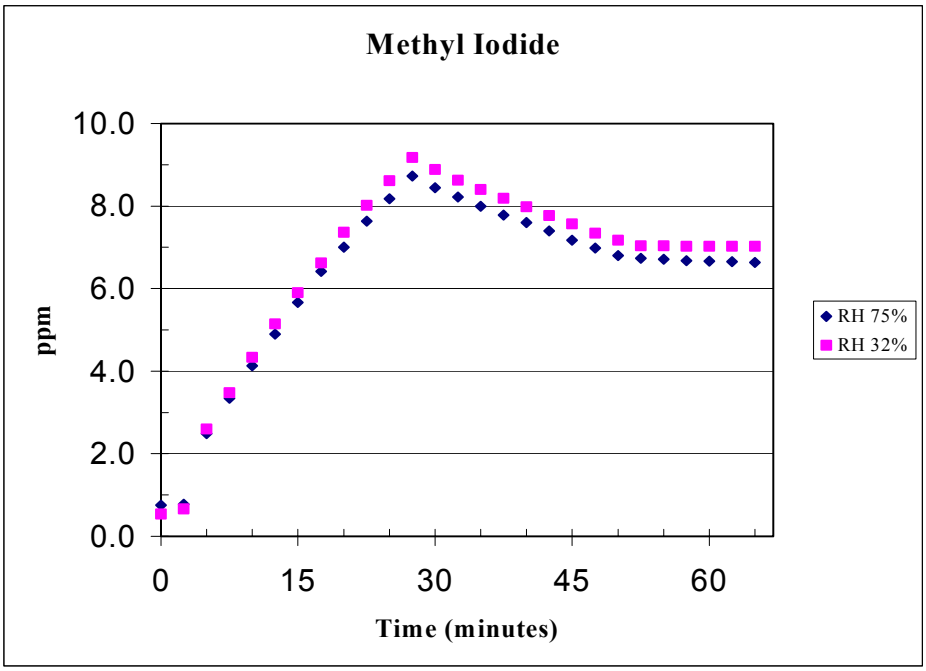

Figure 4.3. Generation and depletion curves of CH_3I dispersed to air with 30%RH and 75%RH as determined by gas chromatography. Generation of CH_3I was terminated after 27 min. At 50 min the pressure differential between the internal and external atmosphere was reduced to near zero.

Additional photolysis experiments were conducted in the semi-dynamic chamber at higher target concentrations. CH_3I's photolytic decay after exposure to UV was observed by both GC-ECD and FTIR spectroscopy (Figures 4.5, 4.6). In the IR spectra of Fig. 4.6 one sees not only the decay of CH_3I, but also the formation of CH_3OH. This will be discussed below.

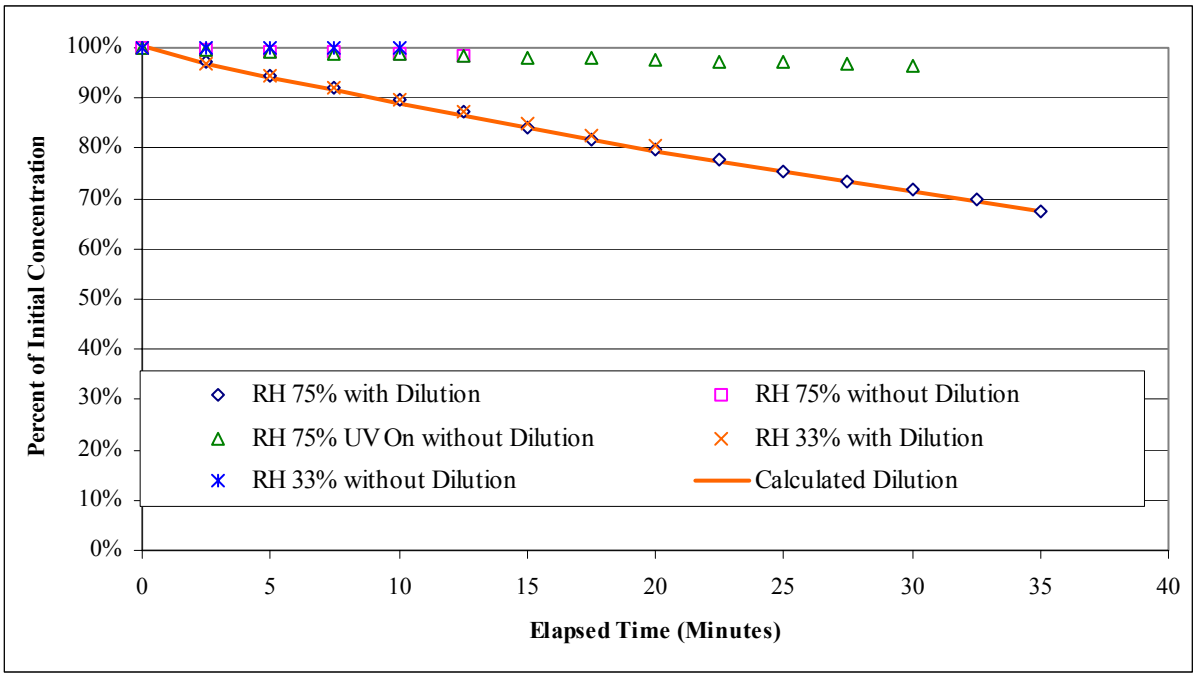

Figure 4.4. Loss of CH_3I in atmosphere of 33 and 75% RH. Loss is calculated as percentage of initial concentration. Some experiments were conducted with no dilution, while others were conducted at a slightly lower tunnel air pressure that caused dilution (modeled as solid line).

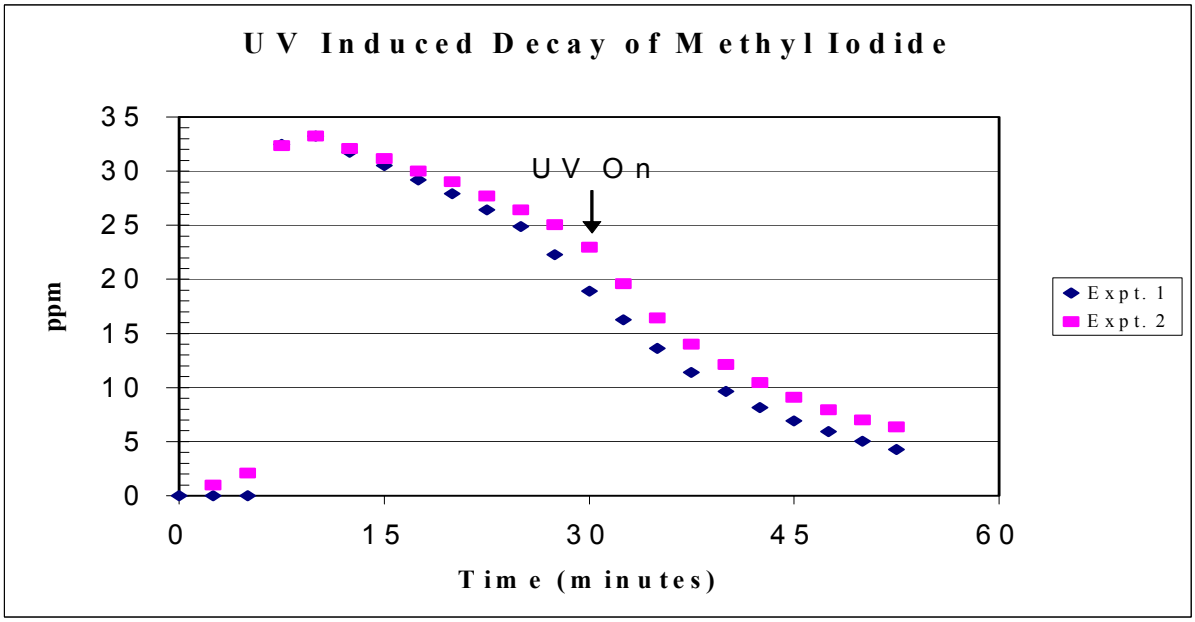

Figure 4.5. CH_3I Analysis via GC: Effect of UV light in the SDC. The simulated sunlight was augmented with UV (emission maximum ~254 nm). The two identical experiments show change in decay rate at ~30 minutes (beginning of the UV exposure). The rate of decay with UV turned on is ~3.5 times the rate of decay under room lights only. SDC was at 20°C, 50% RH.

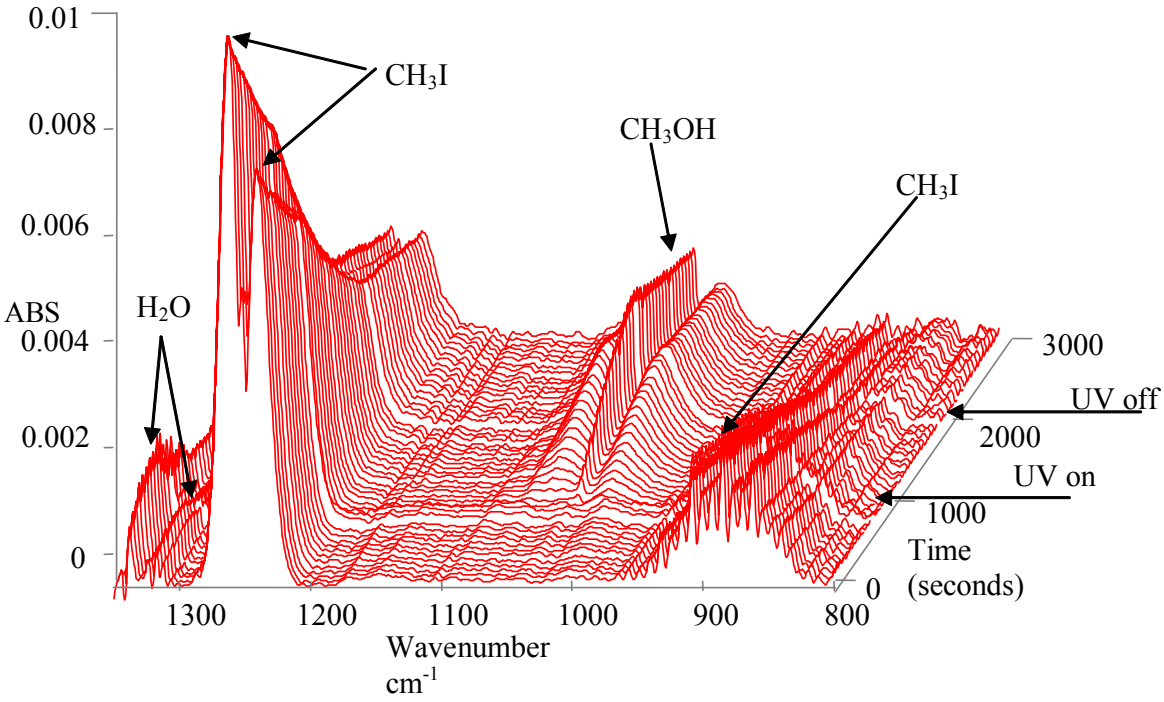

Figure 4.6. Three dimensional stacked dynamic infrared spectra of CH_3I during a UV photolysis test. The spectral resolution was 4 cm^{-1} and the acquisition time for an individual spectrum was ~60 seconds. Methyl iodide introduction into the wind tunnel was stopped at time = 0. Bands due to specific molecules are labeled.

4.5 Data Analysis

To determine the rate of photolysis (j), the difference between rate of loss due to dilution was subtracted from the overall loss rate (dilution plus decay). Using the GC data, the difference between these two data sets is plotted in Figure 4.7.

The experimentally observed loss of CH_3I before and following photolysis for each test was calculated from a plot of the log of the CH_3I concentration (ppmV) vs. time (seconds) and compared to the dilution rate. This loss can be modeled as follows:

$$\frac{d[CH_3I]}{dt} = -k_{dil}[CH_3I] - j[CH_3I] \qquad (4.1)$$

where k_{dil} is the first-order dilution loss rate coefficient and j is the first-order photolysis rate coefficient.

Therefore, the loss, not including photolysis, is

$$\tau = 1/k_{dil} \qquad (4.2a)$$

$$[CH_3I] = [CH_3I]_0 \exp(-k_{dil}\, t) \quad (4.2b)$$

where τ is the observed decay lifetime (seconds) and $[CH_3I]_o$ is the initial concentration of the methyl iodide.

On the other hand, the decay lifetime due to both photolysis and dilution is

$$\tau = 1/ k_{dil} + 1/j \quad (4.3a)$$

$$[CH_3I] = [CH_3I]_0 \exp(-(k_{dil} + j)\, t) \quad (4.3b)$$

and the instantaneous lifetime was calculated as the inverse of the photolysis constant. The rate of loss due to dilution was determined as described in Section 3.0.

The mean lifetime (dilution-only) was $\tau = 57.9 \pm 7.3$ min whereas the lifetime due to dilution plus photolysis was $\tau = 15.1 \pm 0.01$ min, resulting in a mean photolysis rate coefficient (j) for CH_3I of 0.0489 ± 0.0022 min^{-1} (a photolysis lifetime of 20.5 ± 0.9 min). We recognize that this lifetime is specific to this experimental housing and conditions only.

In addition to the GC methods, the loss of CH_3I and the evolution of photolysis product(s) were also seen by FTIR analysis. In Figure 4.6, both the CH_3I peaks near 1250 cm^{-1} and the structured band near 900 cm^{-1} decreased slowly during the first 14 subfiles when the system was illuminated by house lights only. [Note that fluctuations in the water line intensities in the IR region above 1300 cm^{-1}. Although the absorption due to water should ratio to zero if the concentration is the same in the sample and background spectra, small changes in humidity in the tunnel and the laboratory appeared as water absorptions.] When the UV exposure began at the start of the 15th subfile (788 s), a significant increase in the CH_3I depletion rate was observed.

During UV illumination, a secondary peak that eluted before CH_3I was detected by GC-ECD. A similar evolution of a decay product was observed by FTIR spectroscopy. Growth of the new band centered near 1033 $cm^{-1}$was seen after UV exposure was initiated (Figure 4.6). The IR signature of the new compound was compared to reference spectra (Sharpe, 2000) and was identified as that of methanol (CH_3OH). [Note that the early values of the methanol mixing ratios appear slightly negative due to spectrometer noise and spectrometer baseline drift (Figure 4.8)]. The concentration of methanol was monotonically increasing, but cannot be plotted on a logarithmic axis due to the initial negative concentration values. As seen in Figure 4.8, total CH_3I loss was about 50 ppmV during the photolysis period. Adjusting this value to account for the loss due to dilution, the estimated total CH_3I loss during photolysis was 15 ppmV. This compares closely to the estimated 13 ppmV of methanol that was formed during the same period. The exponential constants for the CH_3I decay and the CH_3OH formation are approximately the same (-7.62×10^{-3}, $+9.13 \times 10^{-3}$, respectively). That they are not in perfect agreement is understandable since we have neither accounted for all loss mechanisms nor all sources of CH_3OH.

The decay of the methyl iodide and concomitant growth of methanol after the onset of photolysis can be seen more clearly by integrating the peaks to determine the mixing ratios (Figure 4.8). Once the UV exposure started, the more rapid rate of decay could be seen in the plot (Figure 4.8A). This UV-induced increased decay rate is better clarified in Figure 4.8B where the CH_3I mixing ratio has been plotted on a logarithmic scale. The instantaneous increase in the CH_3I decay rate with UV photolysis after illumination with UV light at 254 nm was -0.0268 ± 0.0031, a 3.5 fold greater rate of loss than that due only to maintaining the test system under slightly negative pressure, i.e. the loss rate due to dilution alone.

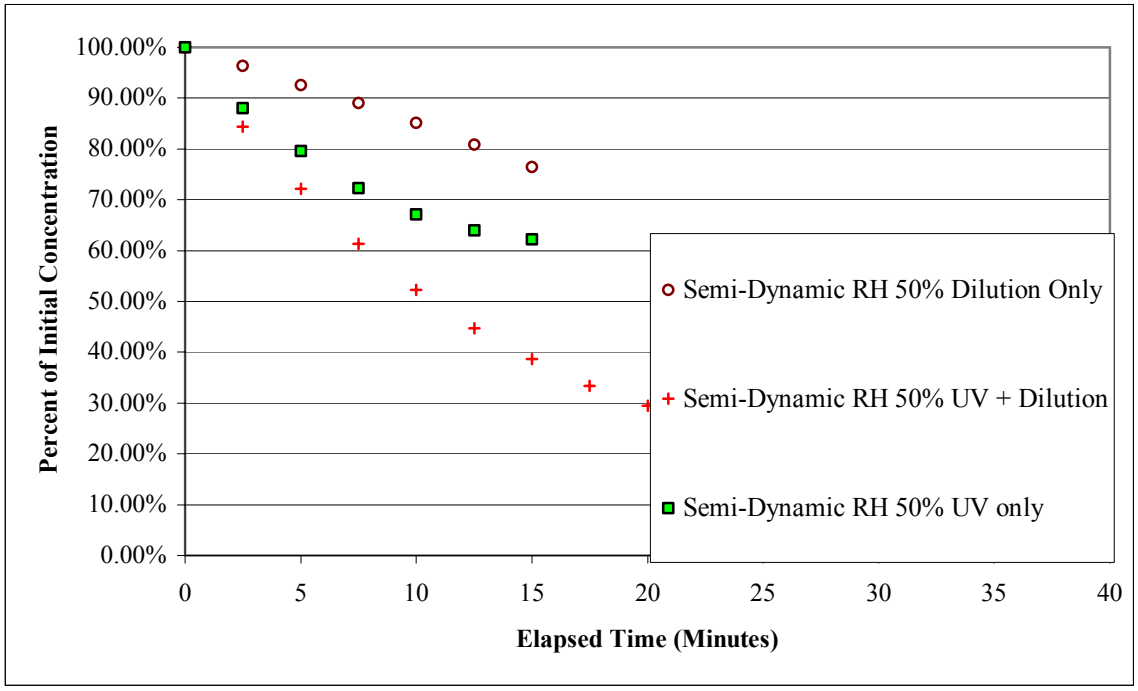

Figure 4.7. Loss of CH_3I during UV photolysis plotted as the difference between the concentrations measured under house lights (dilution due to maintaining a negative pressure in the system but with no UV induced decay) and the concentrations measured under UV illumination.

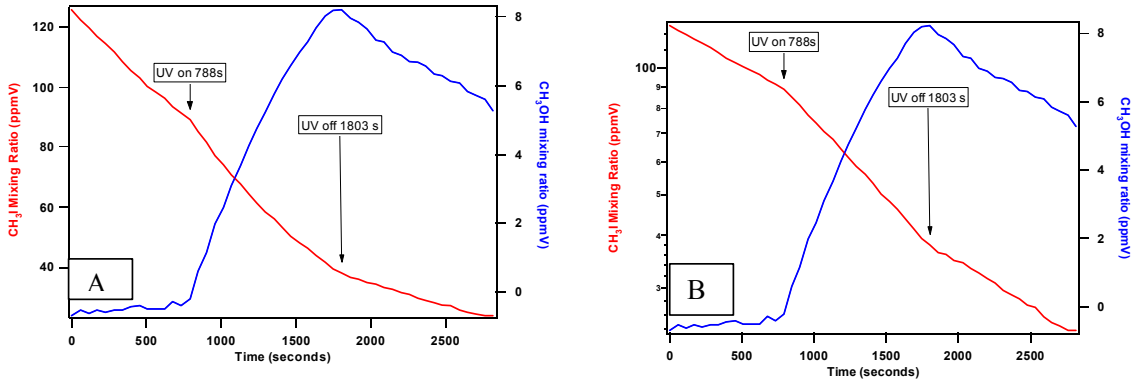

Figure 4.8. Mixing ratio versus time for methyl iodide and methanol from the methyl iodide photolysis based on the FTIR spectra of Figure 4.7. The left axis of (A) is the CH_3I decay and of (B) is a log scale of the CH_3I decay. The MeOH mixing ratio is linearly scaled on the right axis.

4.6 Discussion

We observed no significant changes in CH_3I concentrations due to humidity, wall effects or irradiation with long wavelength UV/Visible light ($\lambda > 290$ nm) during near-field transport simulations. However, photodissociation of methyl iodide was rapid ($j = 0.04889 \pm 0.0022$ min^{-1})

when illuminated with Hg-arc ultraviolet lamps (λ = 254 nm). This rate is comparable to photodissociation rate constants calculated for CH_3I at high altitudes (>50 km) (Roehl *et al*. 1997). Photodissociation rates at these altitudes are of interest because of the potential rapid transport by convective clouds ("Staubsauger" mechanism) of chemicals from low altitudes to the upper troposphere or lower stratosphere (Chatfield and Crutzen 1990). This transport mechanism is particularly important in the tropics. In the boundary layer, photolysis of CH_3I is limited to the spectral region above 290 nm and, thus has much slower rates of decay (2 to 5 day instantaneous lifetime) (Roehl et al 1997).

Methanol (CH_3OH) was identified as a major photolytic product of CH_3I in the test system. In general, many atmospheric mechanisms for the oxidation of methane or halomethanes result in the formation of formaldehyde. Generation of methanol may be a function of the relatively high initial concentration of CH_3I resulting from exposure to UV below the 290 nm region. Appendix A describes a probable decay mechanism resulting in the production of methanol.

Interference from water vapor somewhat hindered quantifying CH_3I by FTIR spectroscopy at low, but field-relevant concentrations (Chameides and Davies 1980). However, the presence of the strong Q-branch of the 1250 cm^{-1} band provided a sufficient signature so as to identify the compound in even high humidity situations. In light of these data, a potential method that may be capable of detecting trace levels of the iodide with greater sensitivity is the application of a novel quantum cascade laser as an optical probe source for CH_3I. This potential technique could also be applicable to detection of thionyl chloride, which has a similar distinctive band (Kelly, 2001).

5.0 Methylphosphonic Dichloride Experiments

A series of experiments with a known reactive chemical, methylphosphonic dichloride (DCMP) were also run in the SDC. No significant effects due to temperature or light exposure were observed. However, DCMP decomposition was strongly coupled with relative humidity. DCMP also demonstrated the suitability of the SDC for use with toxic materials and provided information on the near-field decay of phosphorous-containing compounds.

5.1 Generation of Methylphosphonic Dichloride Vapor

The DCMP experiments were performed in the SDC system as described in Section 2.1. The targeted concentration of DCMP vapor in the SDC was 20 ppmV. Corresponding chemical analyses of the vapors within the system were performed in-time using FTIR, GC, and GC/MS. Because of its reactive/toxic nature and a vapor pressure of ~30 mm-Hg at the melting point of ~35°C, neat DCMP[26] was handled in a vented glove box outside the test system. To generate and deliver methylphosphonic dichloride vapor to the SDC system a simple assembly made of glass, stainless steel and Teflon®, shown in Figure 5.1, was used.

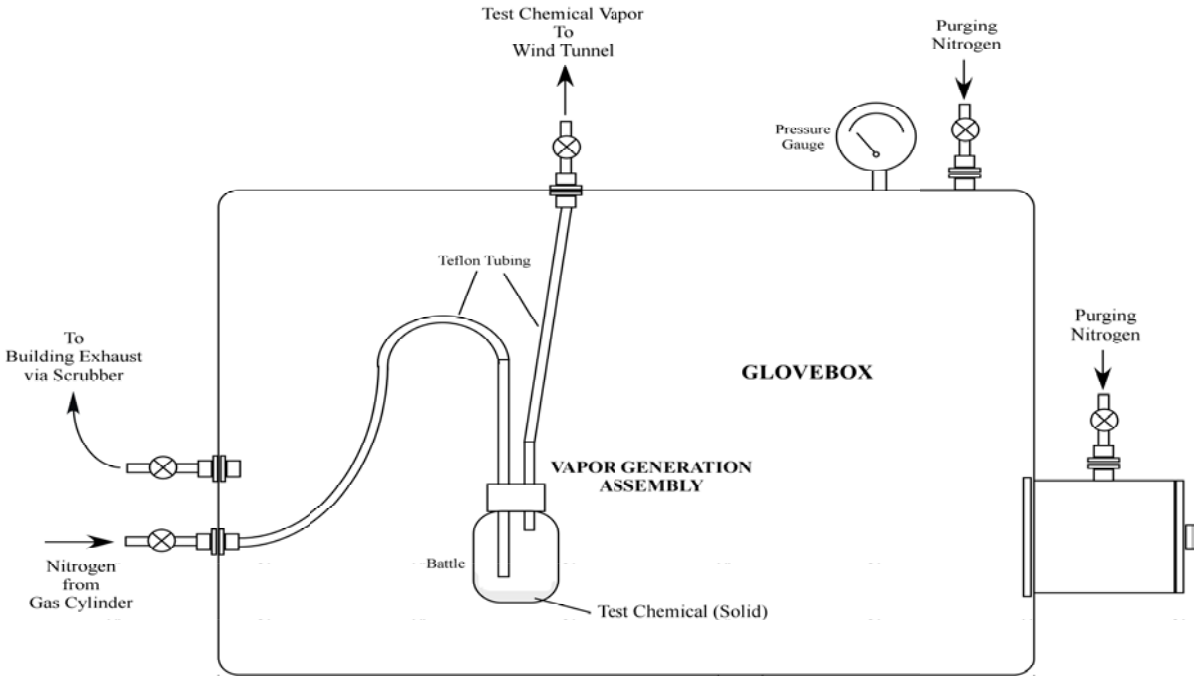

Figure 5.1. Methylphosphonic dichloride vapor generation system.

The glove box was purged with dry nitrogen for ~25 minutes to eliminate residual moisture (final RH <3%) at the beginning of each test day. During this time, the stock bottle of DCMP which had been placed within a previously nitrogen flushed plastic bag was opened within the bag and its interior also purged with nitrogen. An aliquot of the neat DCMP was then pipetted into the vapor generation assembly bottle shown in Figure 5.1.

[26] Aldrich Chemicals, Milwaukee, Wisconsin, 98% purity, CAS #676-97-1

Nitrogen carrier gas[27] was passed through the headspace of the bottle and carried the DCMP vapor to the semi-dynamic system. The concentration of DCMP in the SDC was controlled by adjusting the N_2 flow rate and delivery time. After DCMP was delivered, the delivery line was purged with nitrogen to ensure no DCMP would get into the test atmosphere during the tests. The DCMP/N_2 mixture was injected into the test system at a known temperature and relative humidity, and stirred by two fans to achieve sample homogeneity. This method allows safer handling of the compound, but the rate coefficients must therefore be extracted indirectly as described below. Tests with DCMP were performed at ~23°C and relative humidity levels that included 4, 8, 35, 48 and 75% RH. There was no air change in the SDC system during a test to keep the atmosphere (especially RH) stable.

5.2 GC and GC-MS Analysis of Methylphosphonic Dichloride

Gas chromatography was used to monitor the concentrations of DCMP and potential breakdown products in the wind tunnel. The column used was a DB wax column[28] 15 meters long, 0.53 mm I.D., with a 1.0 micron film. The GC was run at a constant temperature of 40°C. With this configuration the DCMP peak eluted at about 2 minutes. The total time for each chromatogram was approximately 3 minutes, which allowed a time for repetitive measurements of 3.5 minutes, including sample acquisition time and dead time. GC data were acquired simultaneously with the FTIR data to ensure identical atmospheric conditions (such as temperature, humidity and gas concentration). The only peaks other than DCMP observed in the chromatograms were those of water and oxygen, the water peak scaling with the humidity in the tunnel. The observed decay rate of the DCMP by the GC appeared slightly longer than that of the FTIR because of the dead volume involved in the sampling system.

Chemical composition of the atmosphere in the wind tunnel was also evaluated using the HP GC-MS system described in Section 2.2.2. The GC column was a Restek Rtx 502.2, 30 meters long, 0.32 mm I.D., with a 1.8-micron active layer. The data acquisition sequence used was an initial injection of 5 ml of air sample onto the column held at 40°C. After 3 min the temperature was increased to 225°C over a 10-minute period. Prior to the introduction of DCMP, only a few low intensity peaks were observed in the total ion gas chromatogram, none of which had a mass spectrum corresponding to DCMP. This was true under all conditions used in the wind tunnel experiments. Subsequent measurements of the background air in the wind tunnel, the water in the tunnel humidification system and the DCMP introduction system showed that the same GC-MS peaks were present at low levels, primarily from the sample introduction system. The levels of these contaminants did not change over any measurement, were at sub-parts-per-million levels, and did not have an impact on the DCMP studies. Work subsequent to the wind tunnel studies revealed that DCMP required a higher column temperature for more effective elution using the present GC column chosen for the GC-MS.

The GC-MS instrument was calibrated with solutions of DCMP in chloroform at concentrations ranging from 1 to 100 ppm by mass. DCMP was found to elute at 5.2 minutes and the mass spectrum was in excellent agreement with mass spectra in the NIST library. One mL gas samples were withdrawn from the wind tunnel in a one mL gas syringe and manually injected into the GC-MS prior to introduction of DCMP, immediately following introduction, and at about 10-minute intervals. The strongest peaks in the GC/MS spectra were clearly due to DCMP. Additional peaks

[27] Oxarc, Spokane, Washington, purity >99.99%
[28] J&W Instruments, Folsom, California

were observed at later sample times but could not be definitively assigned. Presumably they are due to the same hydrolysis products observed in the IR spectra, but conclusive assignments could not be made.

5.3 FTIR Analysis of Methylphosphonic Dichloride

Figure 5.2 shows the infrared reference spectrum for DCMP (Sharpe, 2001). DCMP has three significant IR bands in the long-wave atmospheric window located at 757, 897, and 1308 cm^{-1}. Figure 5.3 shows a 3-D plot of spectra as a function of time that indicates essentially no change in DCMP concentration at low RH (3%).

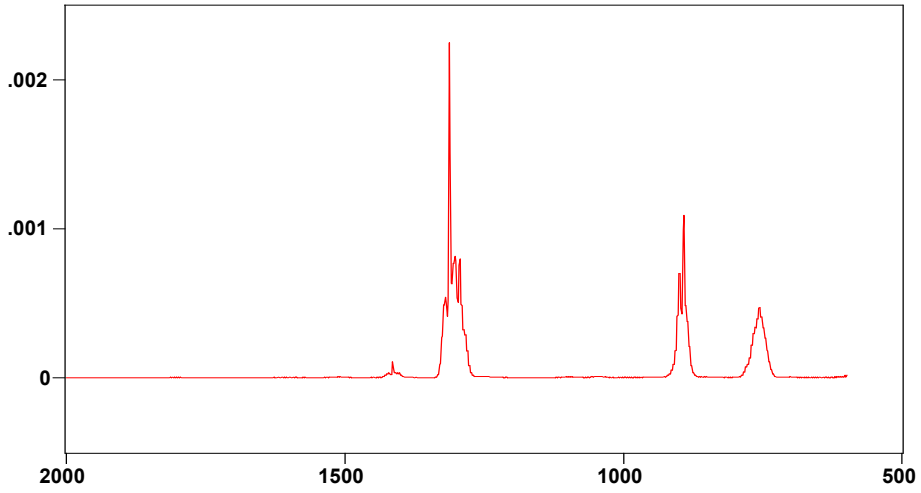

Figure 5.2. Reference spectrum for DCMP from PNNL Infrared Data Base.

The band at 1308 cm^{-1} is slightly prone to interference from adjacent water lines, depending on the change in relative humidity during the course of the measurement. In spite of this possible interference from water, the band at 1308 cm^{-1} was the favored band for monitoring DCMP concentrations because an absorption band of one of the observed decay products overlapped the 897 cm^{-1} parallel band (*vide infra*, Figure 5.4). Both the 1308 cm^{-1} and the 897 cm^{-1} bands displayed narrow and well resolved features; therefore, the resolution for the DCMP studies was increased to 4 cm^{-1}. The water lines near 1600 cm^{-1} and the CO_2 band near 2350 cm^{-1} in Figure 5.4 are due to water/carbon dioxide concentration changes outside the tunnel and hence are simply spurious signals for these studies.

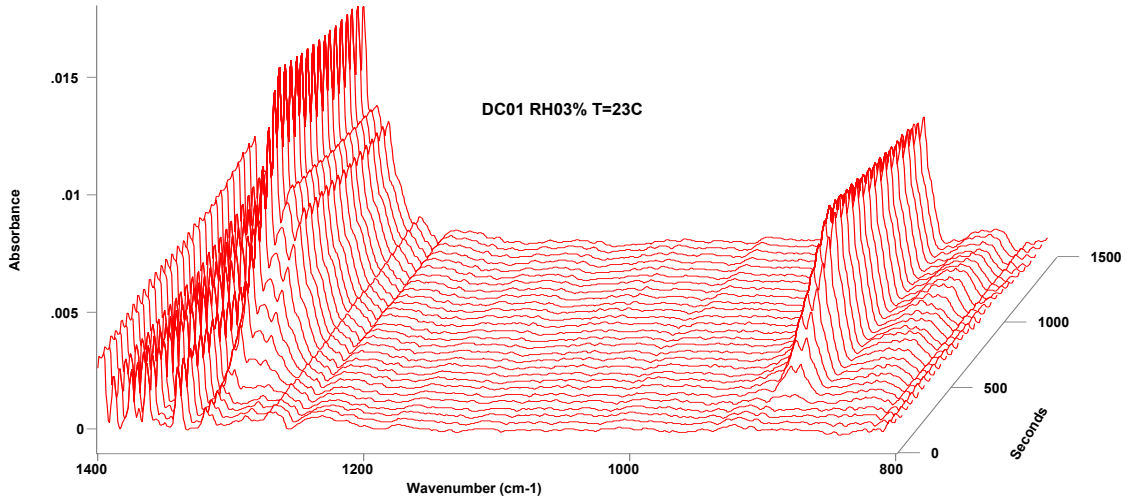

Figure 5.3. 3D stacked dynamic infrared spectra of methylphosphonic dichloride during a 3% relative humidity test. Note the minimal decrease in DCMP concentrations after generation of DCMP ceased (718 s).

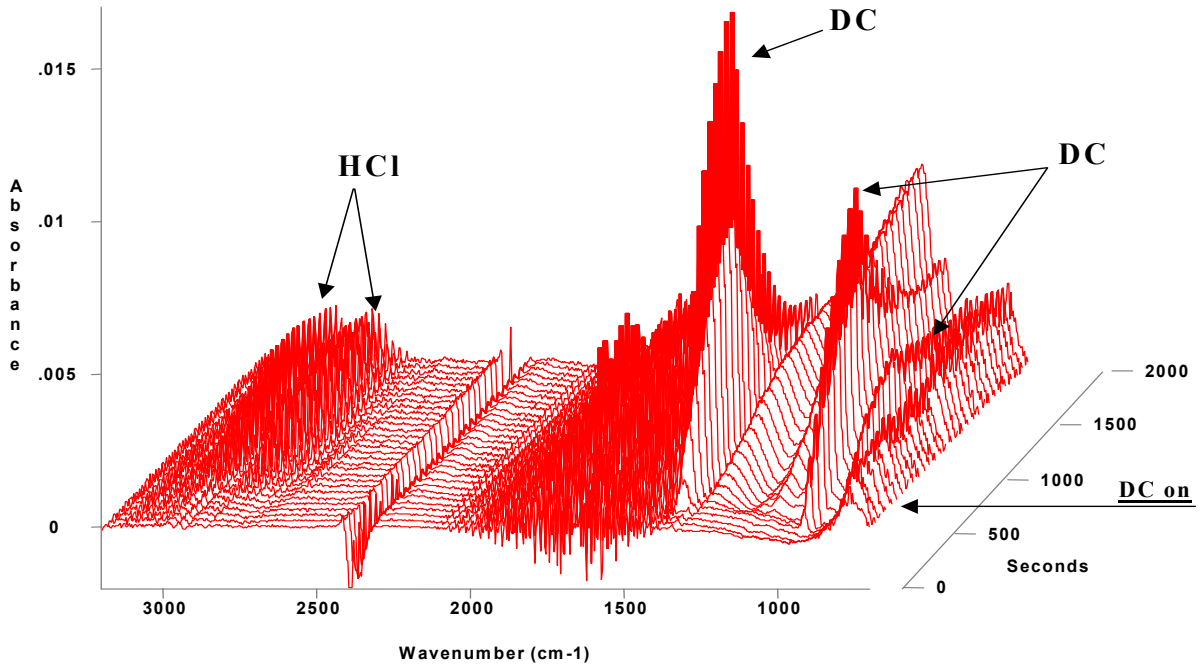

Figure 5.4. 3D stacked infrared spectra of methylphosphonic dichloride (DCMP) and its decay products at about 50% humidity and 23° C. The acquisition time was ~52 seconds/ spectrum. Note the rapid decrease in DCMP concentration after generation was halted (~1280 s).

Other FTIR experimental parameters were similar to those described in pinacolyl alcohol and methyl iodide tests with the exception that the number of individual interferograms per spectrum

(subfile) was reduced to 200 in the DCMP tests to improve the time resolution to less than 1 minute per spectrum. The detection limit for DCMP was approximately 300 ppbV. However, at such low concentrations, the measurement using the 1308 cm^{-1} band was especially susceptible to fluxes in the water vapor concentration exterior to the wind tunnel (see Figure 2.3). The detection limit using the 897 cm^{-1} band was about 600 ppbV, but decay products at times interfered at this wavelength (see Section 5.4).

5.4 Results

In the initial test atmosphere of ~50% RH, a rapid exponential depletion of the parent compound was observed after cessation of DCMP input into the SDC system (Figure 5.5). In subsequent tests, DCMP vapor was introduced into atmospheres at 4%, 8%, 35%, 48% and 76% RH, as shown in Figure 5.6. These data clearly show that the rate of DCMP decay is dependent on the amount of water vapor in the atmosphere into which the compound is introduced: the higher the water concentration, the faster the rate of DCMP decay.

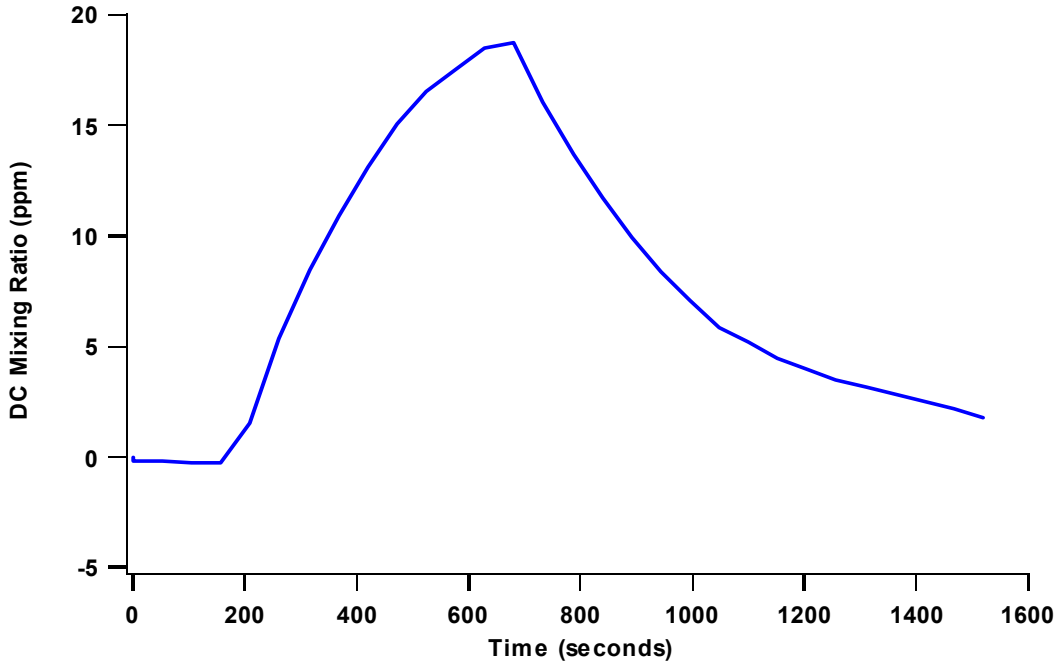

Figure 5.5. Mixing ratio versus time curve for DCMP concentration derived from the infrared spectra at 50% RH. The input flow of methylphosphonic dichloride was stopped at ~700 seconds.

Another effect can also be observed in Figure 5.6. At higher RH (48%, 76%), the achieved concentrations of DCMP were lower than the other studies, even though the same amount of DCMP was injected into the system. The explanation is straightforward, namely that the DCMP was being rapidly hydrolyzed as it entered the SDC chamber. At high RH, the rate of depletion nearly equaled the injection rate, and it was more difficult to build up concentrations of the same magnitude as the low humidity experiments.

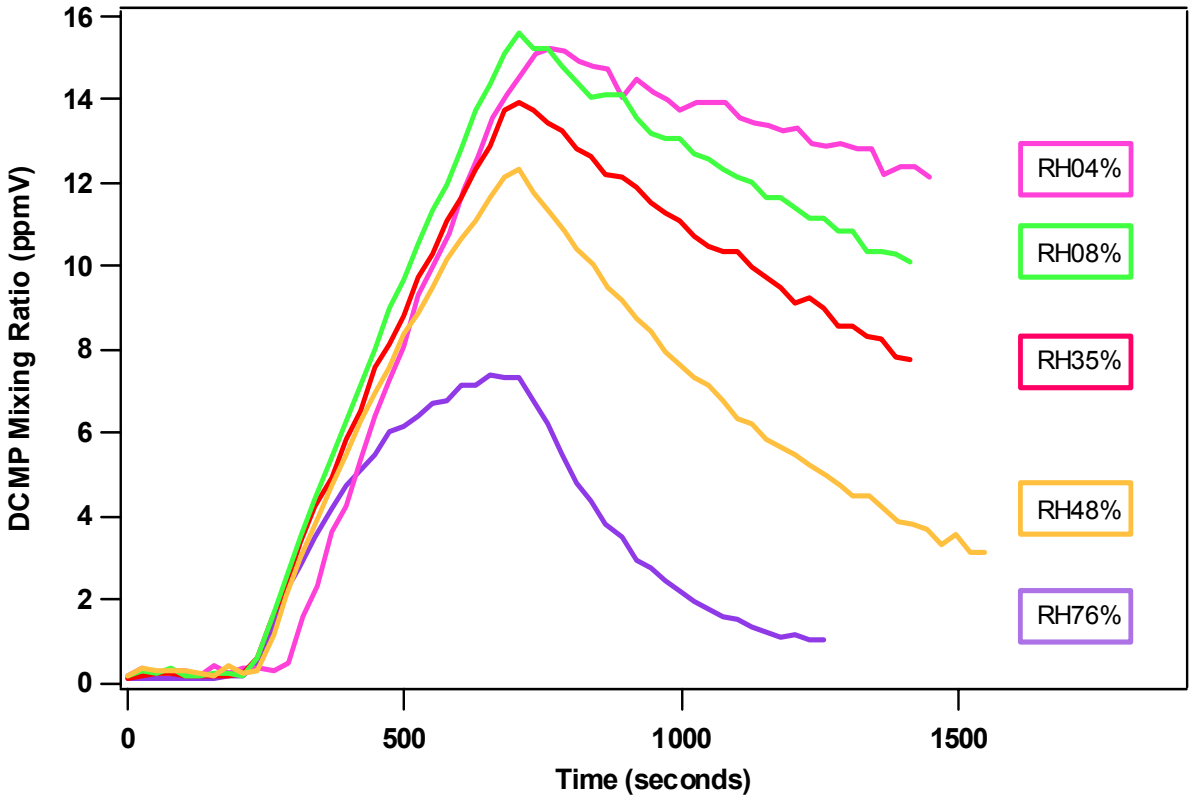

Figure 5.6. Multiple methylphosphonic dichloride decay curves as a function of relative humidity.

Careful inspection of Figure 5.4 also shows decay compounds were observed in the infrared spectra. In atmospheres with significant humidity (>30% RH), these hydrolysis product peaks first appear in the long wavelength region of the infrared about 1 to 2 minutes after the introduction of the DCMP (Figure 5.7). It is important to note that the detected decay peaks correspond to *losses* of e.g. >1 to 5 ppmV *of the parent compound*, which would correspond to concentrations of 1 to 5 ppmV of the daughter compound, assuming a 1:1 stoichiometry of the parent OP to the product phosphorous moiety. To be sure, the chemistry *begins* happening on a much shorter timescale, the 1 to 2 minute corresponds only to the timescale of the reaction to build up concentrations above the detection limit of the current spectrometer system.

Figure 5.8 shows an expanded plot of the MWIR region from the same data of the same experiment as that shown in Figure 5.7. In this high humidity (RH 76%) experiment a product is evolved with a monotonically increasing growth curve. In the MWIR the growth curve is easy to recognize as the parallel band of hydrogen chloride. This was easily verified by comparing to the HCl reference spectrum shown in Figure 5.9. DCMP is known to readily hydrolyze forming HCl as one of the hydrolysis products (Neimysheva *et al*. 1968). Both HCl and the products that evolve in long-wavelength region appear to have similar formation rates (indicating that $k_{formation}$ is similar for these compounds or possibly that the different bands all arise from the same compound).

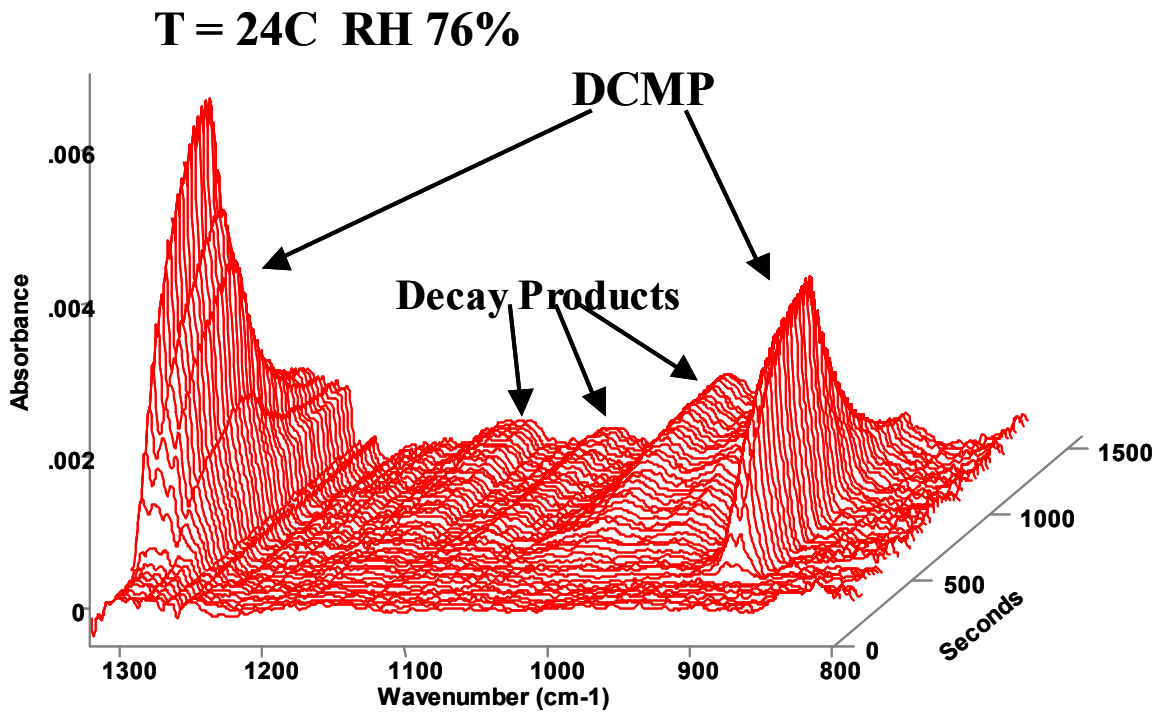

Figure 5.7. 3D stacked infrared spectra of DC and its decay products during the 76% RH study in the long-wavelength region of the infrared. The resolution was 4 cm^{-1} and the spectral acquisition time was ~52 seconds per spectrum.

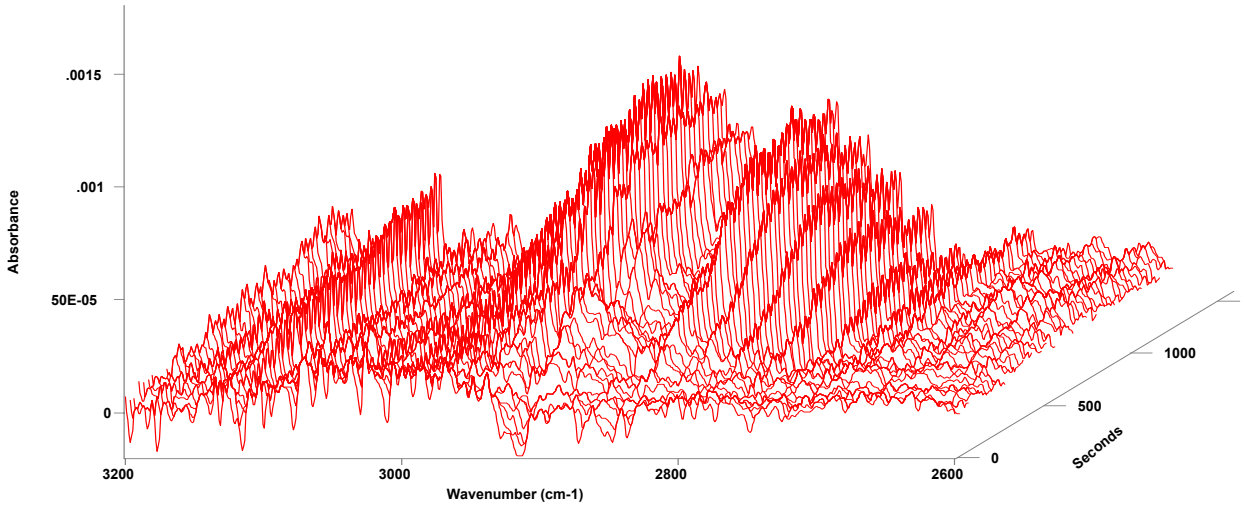

Figure 5.8. 3D stacked infrared spectra of DCMP and its decay products during 75% RH tests in the mid-wavelength region of the infrared. These data are from the same study as Figure 5.7, only displayed in a different wavelength region to show the formation of HCl as a decay product.

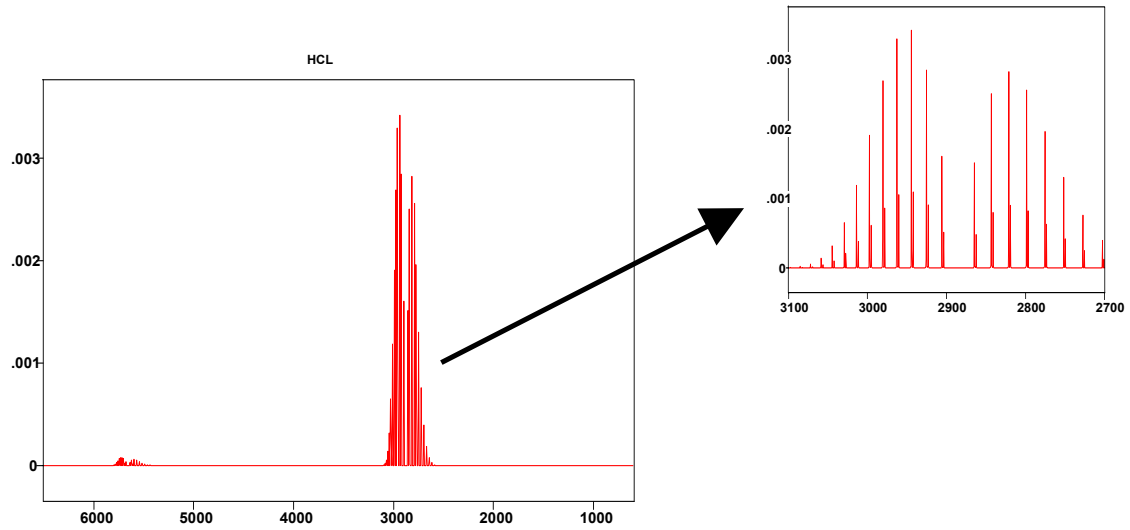

Figure 5.9. HCl reference spectrum from PNNL Infrared Data Base. Compare the distinct parallel band signature centered at 2886 cm^{-1} to the experimental spectra in Figure 5.8.

While the products appeared quickly in both the long-wavelength and mid-wave IR regions, the formation rates were a function of the relative humidity of the chamber atmosphere. In the 48% RH (Figure 5.10) and 75% (Figure 5.7) tests, the product peaks were seen 100 seconds and 50 seconds after the first DCMP peak, respectively.

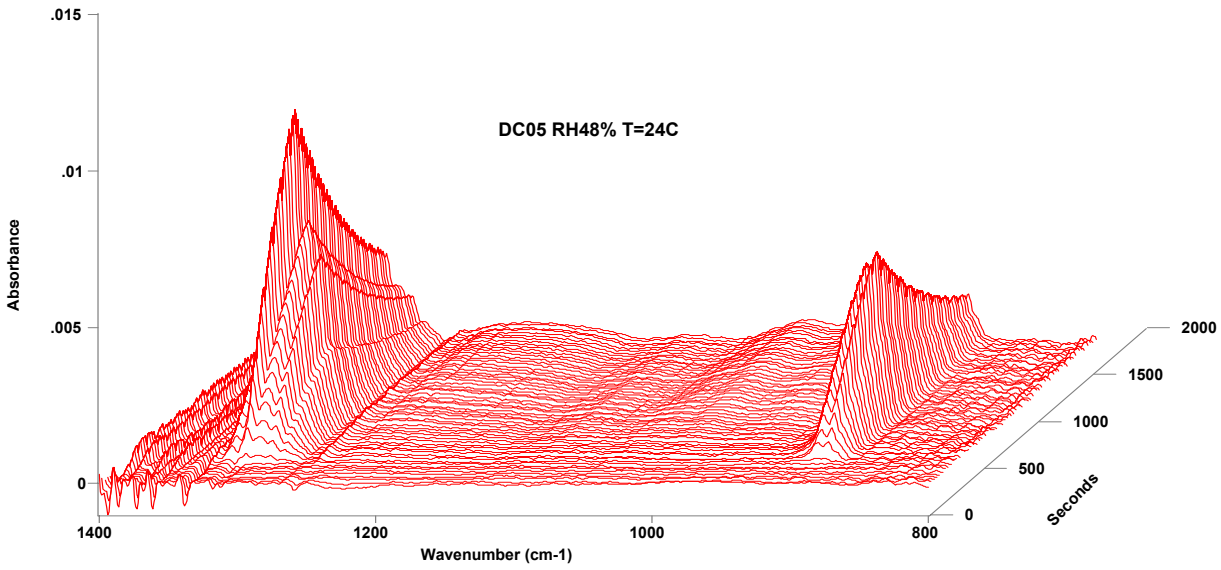

Figure 5.10. 3D stacked infrared spectra of methylphosphonic dichloride (DCMP) and its decay products at moderate (48%) humidity and 24º C. The spectral acquisition time was 24 seconds.

5.5 Data Analysis for DCMP

The specific IR bands used for DCMP analysis as well as the clearly resolved ro-vibronic lines of the band at 2886 cm^{-1} show that both the DCMP reactant and the HCl product are in the gaseous phase. Since DCMP is known to hydrolyze in the liquid phase, one reaction to explain the observed data would be:

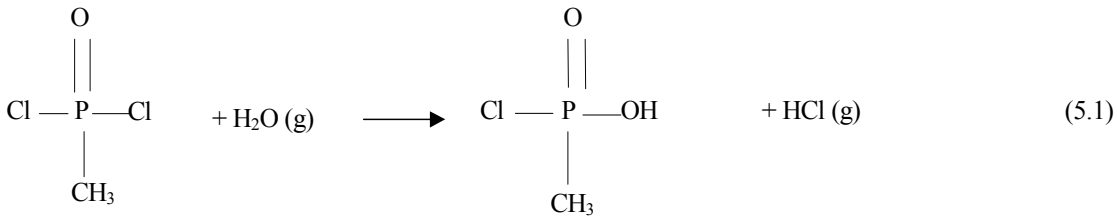

(5.1)

DCMP Methyl Phosphonochloride

Although we have not proposed a specific mechanism, the above reaction clearly explains the consumption of DCMP, the formation of HCl gas, and the approximate observed reaction rate (e.g. 1st or 2nd order) depending on DCMP(g) and HCl(g) concentrations. Since the DCMP is known to readily hydrolyze losing a chlorine atom, it would be logical to propose a second follow-on reaction that forms methyl phosphonic acid:

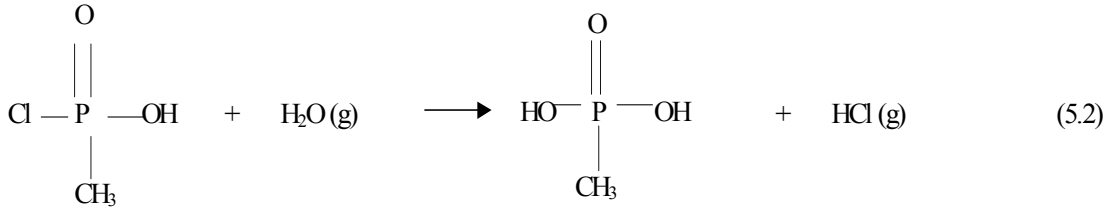

(5.2)

Methyl Phosphonochloride

Methyl Phosphonic Acid (MPA)

The broad peaks due to formation products observed in the long-wave infrared ranging between 900 and 1200 cm^{-1} are thus presumably due to either the methyl phosphonochloride or methyl phosphonic acid degradation products. These bands cannot be definitively assigned at this time due to the lack of reliable gas-phase infrared reference spectra.

Further complications arise due to the low vapor pressure(s) of our suggested formation products. Although DCMP has reasonable vapor pressure (approximately 30 Torr at the melting point of 35°C), the products would be presumed to condense due to their very high melting points (MPA, m.p. = 104°C). In light of this, it is possible that the very broad peaks seen in the IR spectra at later times are the phosphorous moiety formation products that have condensed on the windows, either neat or as constituents of water aerosols.

It is difficult to discuss the kinetics using the appearance of formation products, but some analysis is possible by monitoring the decay rates of the DCMP parent. Specifically, we can use the

hydrolysis decay curves of Figure 5.6, each recorded at a different humidity. Each of these curves can be well fit by a single exponential decay. The DCMP concentration (mixing ratio), C, at time t can be fit by an expression of the form

$$C = A_1 + A_2 \exp(-A_3 t) \quad (5.1)$$

where A_1 is a time offset, A_2 is the peak (maximum) DCMP concentration and A_3 is the overall decay rate for DCMP. Table 5.1 summarizes the concentration equations at various relative humidities. These equations are derived from the data shown in Figure 5.6

Table 5.1. Equations Express DCMP Concentration as a Function of Time.

Relative Humidity	**DCMP concentration (ppmV)**				
04%	C	=	7.3412	+	13.12exp(-0.0006832)t
08%	C	=	3.0329	+	22.12 exp(-0.00080982)t
35%	C	=	-0.12255	+	25.28exp(-0.00082091)t
48%	C	=	-0.14955	+	39.185exp(-0.0016193)t
75 %	C	=	0.29709	+	184.36exp(-0.0045759)t

Only two reactions will be assumed important in describing the decay of DCMP in each experiment. They are shown in Figure 5.11 and are given as reactions 5.1/5.2 and 5.3:

$CH_3Cl_2PO + H_2O \rightarrow (k_h)$ $CH_3P(O)OHCl + HCl$ (5.1)

$CH_3P(O)OHCl + H_2O \rightarrow$ $CH_3P(O)(OH)_2 + HCl$ (5.2)

$CH_3Cl_2PO \rightarrow (k_w)$ Product (5.3)

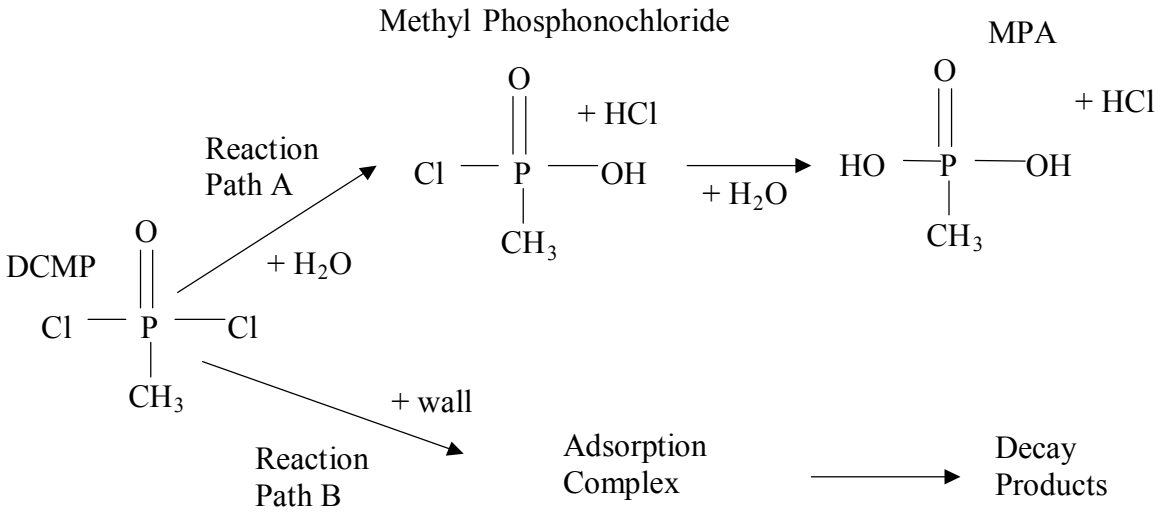

Figure 5.11. Reaction paths and decay products of DCMP.

where reaction path A is the homogeneous hydrolysis described by a second-order coefficient k_h and reaction path B is a first-order loss process used to characterize the reactive and non-reactive uptake of DCMP onto the internal chamber surfaces (i.e., walls) described by k_w.

Because each decay curve in Figure 5.6 is well modeled as an exponentially decreasing function, it is advantageous to write

$$1/\tau_{obs} = 1/\tau_h + 1/\tau_w = k_h [H_2O]^a + k_w \qquad (5.4)$$

where $1/\tau_{obs}$ = the observed decay rate(s)
$1/\tau_h$ is equal to a pseudo first-order rate coefficient $k_h [H_2O]$
$1/\tau_w$ is the heterogeneous wall uptake rate (k_w).
and a is the order of the reaction with respect to water (assumed to be 1)

Our approach is to plot $1/\tau_{obs}$ versus $[H_2O]$ and from a simple linear-regression analysis obtain k_h (i.e., $1/\tau_h$) and k_w (i.e., $1/\tau_w$). A plot is shown in Figure 5.12. From the regression analysis of Figure 5.12, we obtained

$$k_h = 6.0 \pm 1.9 \times 10^{-21} \text{ cm}^3\text{/molecule-s and } k_w = 0.00028 \pm 0.3 \text{ (s}^{-1}\text{)} \qquad (5.5)$$

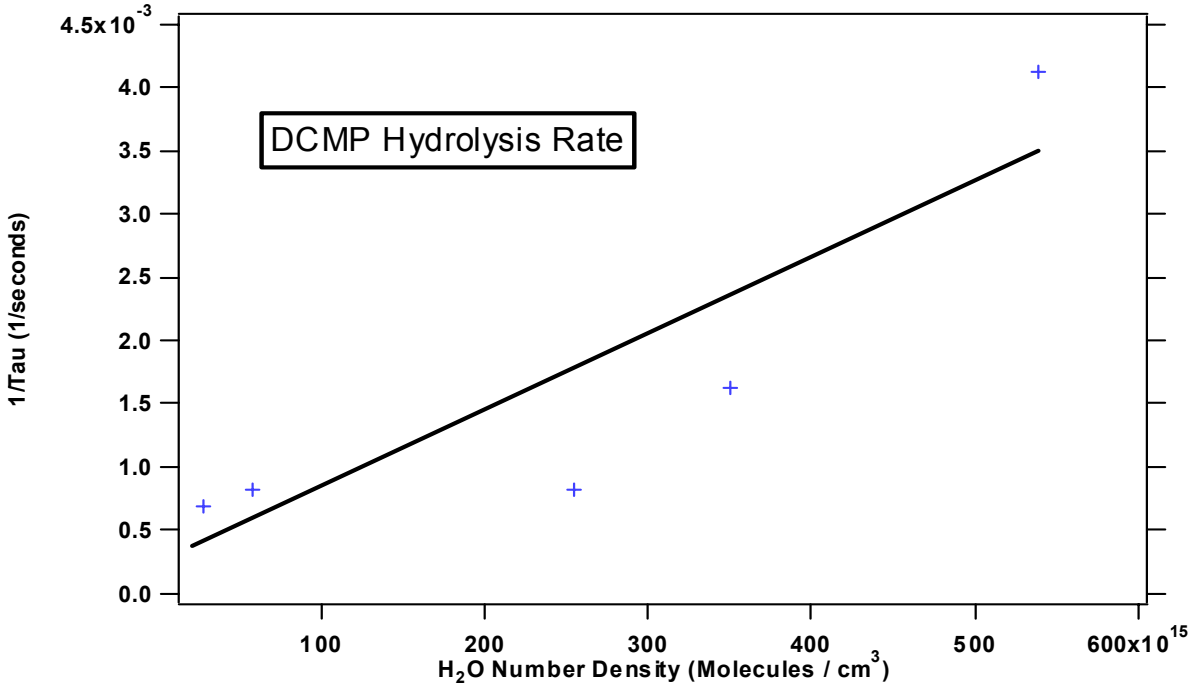

Figure 5.12. Methylphosphonic dichloride reaction rate as a function of water concentration.

The k_h value 6.0 ± 1.9 x 10^{-21} cm^3/molecule-s is easily obtained from the slope of the line in Figure 5.12 and is a reasonable value for a gas-phase bimolecular reaction. Clearly further study is warranted to better determine both k_h and k_w, of this labile species, but the above data are a good first attempt at determining the hydrolysis rate constant. Further discussion is below.

5.6 Discussion

These experiments indicate that the primary environmental decay path of DCMP is via hydrolysis. Dahl *et al*. (1984) have found that under physiological conditions, methylphosphonic difluoride hydrolyzes rapidly to HF and methylphosphonfluoridic acid (MF). Rosenblatt *et al*. (1995) have reported that MF hydrolyzes rapidly forming methylphosphonic acid (MPA) and HF. As a dichloride derivative, DCMP would likely behave in a similar manner, hydrolyzing rapidly to methyl phosphonochloride with this compound further hydrolyzing to MPA. In order to investigate fully the mechanism of DCMP decay, further studies are warranted, but the data generated in these experiments lend credence to postulating a simple hydrolysis (at least as a first step) leading to the disappearance of DCMP(g) and the concomitant appearance of HCl(g), with a clear dependence on H_2O concentration.

Both temperature and UV light-induced decay were relatively unimportant compared to the effects of relative humidity. DCMP exhibited an exponential decay rate whose lifetime was a function of the relative humidity. Compound dissociation was so rapid at high relative humidity (≥80% RH) that sufficient concentrations of the parent chemical could not be attained to permit reliable determination of the decay rate. The rate constant for hydrolysis of DCMP at 296 K was determined to be $k_h = 6.0 \pm 1.9 \times 10^{-21}$ cm^3/molecule-s, resulting in a typical tropospheric lifetime on the order of only a few minutes due to hydrolysis. Decay due to reaction with the hydroxyl radical has been measured by others to be $6.4 + 10^{-14}$ cm^3/molecule-s for an estimated tropospheric lifetime at mid-latitudes of 180 days assuming an average OH radical concentration of 1.0×10^6 molecules/cm^3 (Martin *et al*. 2002). Hydrolysis thus appears to be the predominant decay path in the troposphere.

Concomitant to the gas-phase decay of DCMP, we observed the evolution of several decay products. The MWIR peaks were unambiguously identified as HCl(g). The relationship between the relative humidity and HCl concentrations were complex and may be related to additional decay product reactions and/or liquid phase adsorption. The broad peaks of the formation products observed in the LWIR range between 900 and 1200 cm^{-1} are presumably due to either the methyl phosphonochloride or methylphosphonic acid degradation products. These bands cannot be unambiguously assigned at this time due to the lack of reliable infrared reference spectra of the (transient) species.

Further complications arise due to the low vapor pressures of our suggested formation products. Although DCMP has reasonable vapor pressure (approximately 30 Torr at the melting point of 35°C), the products would be presumed to condense due to their higher boiling and melting points. In light of this, it is possible that the very broad peaks seen in the IR spectra at later times are the phosphorous moiety formation products that have condensed on the windows, either neat or within water aerosols.

6.0 Thionyl Chloride Experiments

Thirty-five experiments were performed in the SDC on thionyl chloride ($SOCl_2$) at two temperatures and multiple humidities. Both the decay of the parent $SOCl_2$ and the growth of the breakdown products were observed. The results presented here are taken from a paper submitted for publication in a peer-reviewed journal (Johnson *et al*. September 2002) and are consistent with previous work.

6.1 Generation of Thionyl Chloride Vapor

Due to its reactive/toxic nature, $SOCl_2$[29] was handled in a vented glove box outside the test system where it was mixed with UHP nitrogen carrier gas[30] and introduced to the test system; all hardware in the mixing assembly was made of either stainless steel or Teflon®. Also, because of the compound's highly toxic and reactive nature, the experiments were carried out using a pulsed-aliquot-kinetic-method (PAKM), whereby a single pulse (typically <35 seconds duration) of the $SOCl_2/N_2$ mixture was injected into the test system at known temperature and relative humidity and stirred by two fans to achieve sample homogeneity. This method allows for safer handling of the compound, but the rate coefficients must be extracted indirectly as described below. These pulse durations typically lasted 15 to 75 seconds, short compared to the compound decay times of ~5 to >60 minutes, depending on water concentration (*vide infra*).

Because the vapor pressure of thionyl chloride is approximately 130 mm-Hg at 20°C, a simple assembly as shown in Figure 6.1 was used to generate and deliver thionyl chloride vapor to the SDC system. The glovebox was purged with nitrogen for ~25 minutes to eliminate moisture (RH<3%) at the beginning of each test day. During that time, the bottle of thionyl chloride was placed in a plastic bag and purged with nitrogen. The flask was also purged with nitrogen. Approximately 1 mL of thionyl chloride was then transferred to the flask for vapor generation.

UHP nitrogen was flowed through the headspace of the flask to carry the thionyl chloride vapor to the SDC. The concentration of $SOCl_2$ in the wind tunnel was controlled by adjusting the nitrogen flow rate and delivery time. After $SOCl_2$ was delivered, the delivery line was purged with nitrogen to ensure no $SOCl_2$ would leak into the test atmosphere during the tests. The inlet nozzle with the $SOCl_2/N_2$ mixture was approximately 20 cm from the probing IR beam, with the fans placed behind the inlet nozzle (see Figure 2.2). The mixing time under these conditions within the large chamber was tested in separate experiments with less reactive compounds and was found to be on the order of 10 seconds.

The original targeted concentration of thionyl chloride vapor in the SDC was 10 ppmV. The concentration was increased to ~50 or 100 ppmV to increase the signal relative to the noise levels. Tests were performed at ambient (24°C) and warm (36°C) temperatures, and multiple relative humidity levels. Thionyl chloride was very reactive and corroded the sensors, thus causing the output signals from the temperature and relative humidity sensors to drift, particularly at high SOC l_2 concentration and high relative humidity. There was no air exchange to the SDC for most tests in order to keep humidity stable. Tests were performed both with UV lights on and off, but no significant photolysis effects were seen.

[29] Aldrich Chemicals, Milwaukee, Wisconsin, 99% purity, CAS #7719-09-7
[30] Oxarc, Spokane, Washington, Purity >99.99%

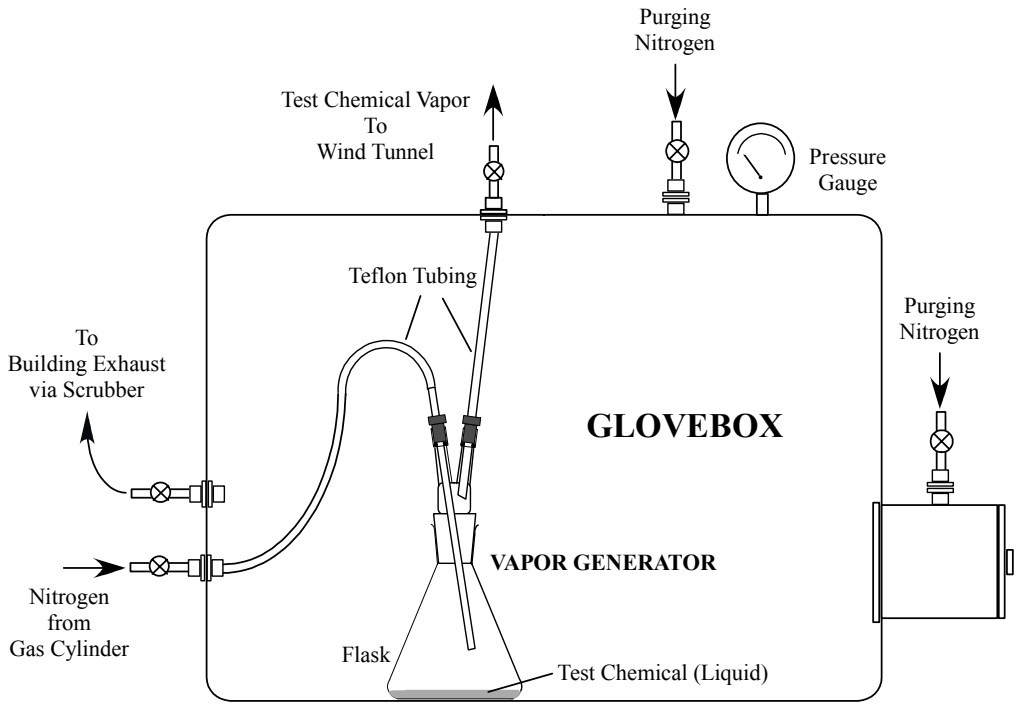

Figure 6.1. Thionyl chloride vapor generation system

6.2 Gas Chromatograph/Mass Spectrometer Analysis of Thionyl Chloride

Chemical composition of the atmosphere in the wind tunnel was evaluated by GC-MS described in section 2.2.2 using a Restek RTX 502.2 GC column 30 meters long, 0.32 mm i.d. and a 1.8 micron active layer. The data acquisition sequence used was injection of 2 ml of air sample onto the column held at 100°C. After 3 minutes the temperature was ramped to 225°C over a 10 minute period. Thionyl chloride was found to elute at 3 minutes under these conditions. The GC-MS system was found to have a linear response using standardized concentrations of $SOCl_2$ in dry air from 5 to 100 ppmV.

The air from the tunnel was sampled in 2 ml aliquots using a 5 cm^3 air-sampling syringe at the beginning, middle and end of each IR data acquisition. The concentrations observed with the GC-MS were in good agreement with those measured with the FTIR. The only breakdown products observed with GC-MS were SO_2 and HCl.

In addition to the hydrolysis experiments conducted in the wind tunnel, ultraviolet/visible (UV/Vis) spectra were recorded in the laboratory[31] with a 9.96 cm electrochemically polished gold-plated cell equipped with quartz windows. Data were recorded from 900 to 190 nm with the slits set to 0.2 mm. The sample was freeze-pump-thawed four times to remove air. Initial experiments evidenced SO_2 as an impurity at approximately a 10% level. In subsequent experiments the SO_2 was removed from the sample by pumping while maintaining the sample at ~ -50°C. UV/Vis spectra were recorded after verifying sample purity by infrared spectroscopy. Rather than record a single spectrum, four different burdens of $SOCl_2$ were recorded and the absorption coefficient

[31] Shimadzu 2501C dual beam spectrometer, Kyoto Japan

determined as the slope of a plot of absorbance versus concentration. The UV/Vis data are reported as the absorbance corresponding to a path length-concentration product of 1 ppmV-m.

6.3 FTIR Analysis of Thionyl Chloride

For the wind tunnel experiments infrared spectroscopy proved to be the most useful technique as it allowed for the simultaneous monitoring of both the parent compound ($SOCl_2$) and the formation of products in a time-resolved fashion. The same MIDAC model M2401-C emission FTIR was interfaced to the tunnel as described in Section 2.2.1. Data parameters are standard for the MIDAC M2401-C and are in accordance with the recommended reporting protocol for FTIR spectroscopic parameters (Bertie, 1998).

The IR reference spectra of $SOCl_2$, SO_2, and HCl were obtained from the PNNL infrared database (Sharpe 2001). Fortunately, the spectrum of $SOCl_2$ has very significant structure in the infrared atmospheric window between 700 and 1300 cm^{-1}. In particular, it has an especially strong band with a narrow Q-branch centered at 1251 cm^{-1}. Hence, the spectrometer was set to 4 cm^{-1} resolution so as to be able to resolve the P- and R-branches of the strongest band; the Q-branch possessed too narrow a linewidth to be fully resolved with the current spectrometer. Concentrations were derived using the Beer-Lambert absorption law as discussed in Section 2.2.1. In the time-resolved experiments, the number of interferogram co-additions was changed depending on the relative humidity of the experiment. Although the spectral resolution (4 cm^{-1}) was the same in all studies, for the high humidity studies fewer interferograms were averaged in order to better capture the fast dynamics, whereas for the lower humidity measurements more co-additions were recorded for each individual "time-slice" spectrum in order to achieve better signal/noise ratios.

6.4 Results

The results of an $SOCl_2$ hydrolysis experiment at high humidity (T = 36°C, 63% RH) are displayed in Figure 6.2. Although a total of 35 such experiments were carried out, the absorption features due to products are more readily visible in a high humidity experiment. The results are displayed as a stacked file with absorbance versus wavenumber versus time, where each "subfile" spectrum represents a time interval of approximately 14 seconds. The infrared spectra reveal several features: First, the $SOCl_2$ band near 1251 cm^{-1} reaches a rapid maximum within two time slices (i.e. less than 28 seconds). [The time intervals prior to introduction of the $SOCl_2$ have not been displayed.] This 1251 cm^{-1} band at longer times then shows a very distinct exponential decay with a 1/e lifetime of 184 seconds.

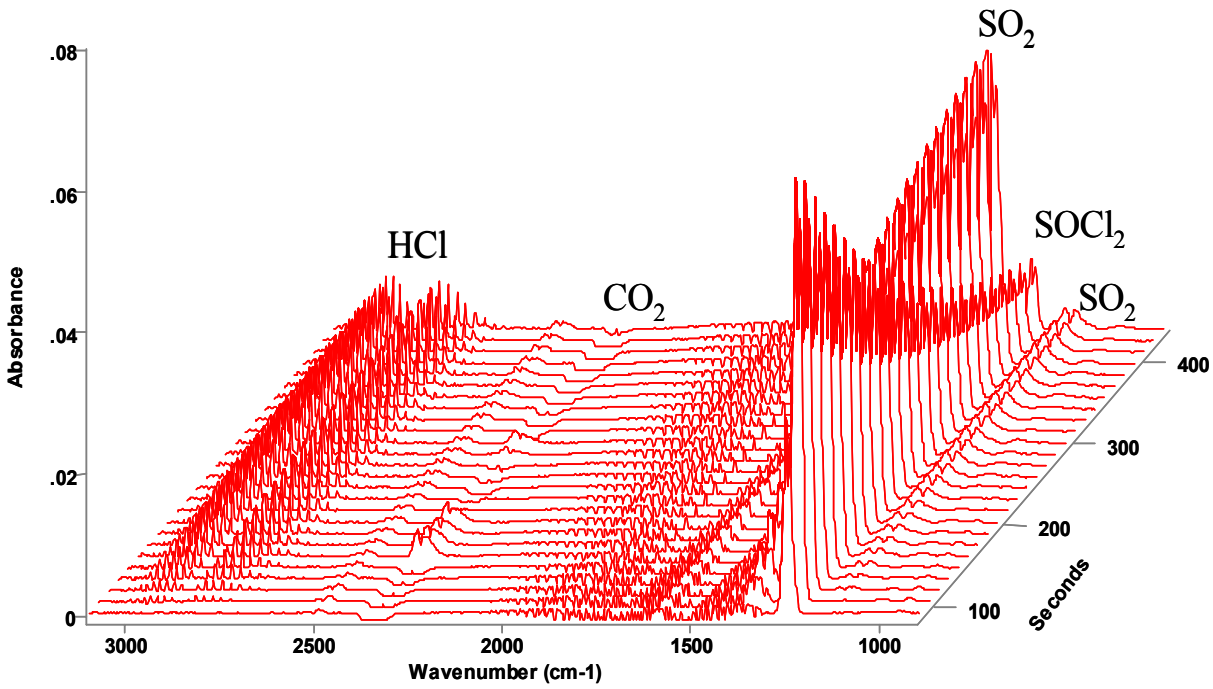

Figure 6.2. 3D dynamic infrared spectra of thionyl chloride hydrolysis during an experiment at 36.5°C and 63% relative humidity. The spectral resolution was 4 cm^{-1} and the acquisition time for an individual spectrum is 14 seconds. Bands due to specific molecules are labeled.

Concomitant to the rapid onset of $SOCl_2$'s decay, we see the formation of SO_2 as witnessed by two bands, the strong ν_3 asymmetric stretch band near 1361 cm^{-1}, as well as a much weaker, broad doublet near 1151 cm^{-1} (ν_1 symmetric stretch) (Herzberg, 1945; Sumpf, 2001). Although the SO_2 ν_3 band is the strongest band, it suffers from interferences by lines in the P-branch of the water ν_3 bending mode, making quantitation somewhat more difficult. In addition to formation of SO_2, the infrared spectra also show the formation of another product, namely the characteristic band of HCl centered at 2886 cm^{-1}. The HCl product is also first observed directly after introduction of the $SOCl_2$, and, similar to SO_2, it also follows a monotonically increasing growth curve. Of lesser importance, one sees variations in the water and CO_2 concentrations as witnessed by the intensity changes in the ro-vibronic lines of the water bending mode near 1604 cm^{-1} as well as the perpendicular ν_3 asymmetric stretch of CO_2 near 2350 cm^{-1}, respectively. The spurious water and carbon dioxide absorptions arise due to the two air spaces between the tunnel and source as well as between the tunnel and spectrometer, as depicted in Figure 2.3. These spaces were not purged; the H_2O and CO_2 signals can thus be ignored as they arise primarily from concentration changes outside the SDC.

Other than the HCl, SO_2, $SOCl_2$, H_2O and CO_2 bands, no other species were observed in the infrared spectra. We also note that the concentrations observed with the GC-MS technique were in good agreement with those measured by FTIR. The only breakdown products observed by either the GC-MS or infrared spectroscopy were SO_2 and HCl. With the exception of H_2, O_2 or Cl_2, infrared spectroscopy should in principle be able to identify all molecular products formed here, provided there is sufficient sensitivity. For these kinetic studies, the molecular mixing ratios were derived by baseline-correcting the individual spectra using a multiple-point baseline fit. The data were then inspected for interferences and integrated over specific regions for each species.

So long as Beer's law is obeyed, the band integral is proportional to the molecular mixing ratio of each species where the absorption coefficient (in $(ppmV\text{-}m)^{-1}$) is determined from the reference spectra. For each spectrum the corresponding mixing ratio is thus derived, where the wavenumber domains used for analysis were as follows:

$$HCl: \ 2884.6 \text{ to } 2711.3 \ cm^{-1} \qquad (6.1)$$

$$SO_2: \ 1397.2 \text{ to } 1315.0 \ cm^{-1} \qquad (6.2)$$

$$SOCl_2: \ 1287.1 \text{ to } 1215.9 \ cm^{-1}. \qquad (6.3)$$

For these experiments, the concentrations of $SOCl_2$, SO_2 and HCl were all derived from the same 3D plot of infrared spectra for the experiment and are displayed versus time. One example of derived mixing ratios is presented in Figure 6.3, but the infrared spectra were in fact converted to concentration data and analyzed for all 35 hydrolysis experiments performed.

In Figure 6.3 we present the results of a 19% RH experiment (T = 36°C). The thionyl chloride concentration rises quickly, having been introduced at approximately t = 83 s and reaches its maximum value by t = 166 s; this is consistent with the pulse injection time which was measured to be 60 ± 2 s for this experiment. After the $SOCl_2/N_2$ flow is switched off, the infrared spectra show that the $SOCl_2$ parent compound undergoes an exponential decay in concentration. For each experiment the data were well fit by a single exponential decay.

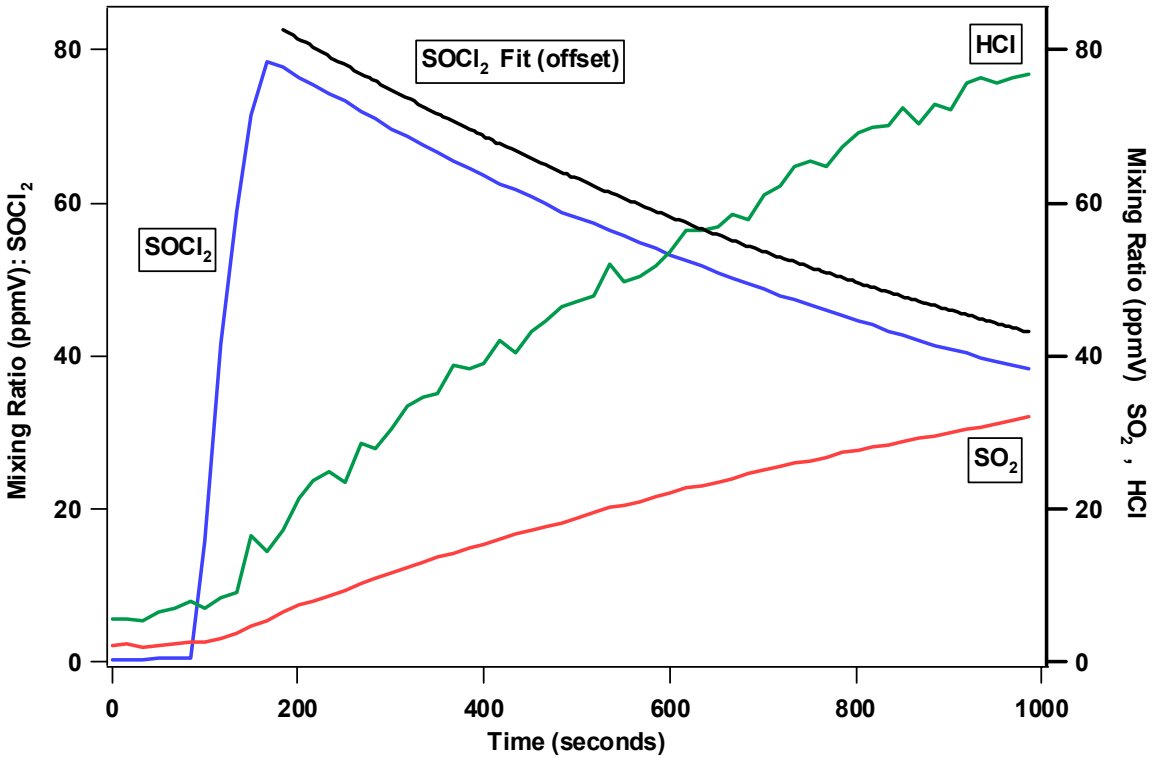

Figure 6.3. Rapid formation and decay curve of $SOCl_2$, along with the growth curve of the SO_2 and HCl products in an experiment at 36°C and 19% relative humidity. The acquisition time for an individual spectrum determines the grid spacing on the time axis. Also shown is a theoretical fit to the $SOCl_2$ decay, which has been offset for clarity.

A single exponential curve was fit to the $SOCl_2$ data in Figure 6.3 in particular, and the fit yielded the following values:

$$C_{SOCL2} = 6.971 + 85.41 \exp(-0.001022 * t) \quad (6.4)$$

where C_{SOCL2} is the $SOCl_2$ mixing ratio in ppmV and the time t is measured in seconds.

The $SOCl_2$ mixing ratio and the theoretical fit to the decay are plotted with the fit data vertically offset for clarity; the agreement is excellent. Of the values in this equation, only the exponential constant ($1/\tau$) is of significance since the offset and pre-exponential terms are determined by when the $SOCl_2$ is introduced and its initial concentration, both of which are easily varied and hence arbitrary parameters. If reproducible, the exponential decay constant should depend only on the temperature and relative humidity (*vide infra*). To test this, the experiment was repeated three times at the same nominal temperature and humidity to determine the reproducibility of the ($1/\tau$) constant. For the three experiments at 36.0 ± 1.0°C and RH 18.0 ± 1.5% the decay constant was found to be ($1/\tau$) = 0.00104 ± 0.00013 (1/s). The parameter τ will be shown below to contain information about the hydrolysis rate coefficient. The greatest source of experimental error was the difficulty in preparing and measuring an air mass this large at constant temperature and relative humidity, exacerbated by the fact that at high humidity the $SOCl_2$ was observed to corrode the temperature/humidity sensor.

Figure 6.3 also displays the formation curves of both SO_2 and HCl, which were obtained from the infrared spectra in the same fashion. The appearance of these two products occurs within the first time interval upon addition of the $SOCl_2$, indicating a rapid onset of reaction. There is also some evidence of SO_2 and HCl, especially HCl, near times t = 0 (i.e. before the $SOCl_2$ has been introduced). This is in part due to the spectrometer baseline drift, and the fact that the software measures all values above the baseline (including noise). In the case of HCl, however, there is another effect manifesting itself. After the $SOCl_2$ reactant was mostly or completely depleted, the SO_2 values remained nearly constant, but the gas-phase HCl absorptions were seen to decrease with additional lapse of time. Since the SDC was sealed, this is ascribed to HCl adsorbing to the walls and/or components inside the Teflon®-lined chamber. It was further observed that after the chamber was purged with fresh air, small concentrations of gas-phase HCl were seen to slowly build up, lending further credence to a sorption/desorption hypothesis. HCl is known to be a very polar molecule with long-lasting memory effects (Fried *et al*. 1984; Harris *et al*. 1992).

This small effect notwithstanding, upon hydrolysis of the $SOCl_2$ it was seen that the HCl and SO_2 were formed simultaneously in a stoichiometric ratio of approximately 2:1 as seen in Figure 6.3. This was observed in each of the 35 experiments performed, and the HCl/SO_2 stoichiometry averaged over 20 of the experiments with significant HCl and SO_2 production was determined to be 1.66 ± 0.45. We observe that the values for the SO_2 and HCl mixing ratios have larger error bars than those of $SOCl_2$ because of their smaller absorption coefficients as well as their greater susceptibility to water interferences.

Figure 6.4 juxtaposes the temporal decays of $SOCl_2$ for four different humidities. All these data were recorded at 36.0 ± 1.0°C, and each trace corresponds to a single experiment at a different humidity: The decay time for thionyl chloride clearly decreases with increasing humidity. The observation that the $SOCl_2$ curves do not all rise at the same time is due to the sample injection time variability among experiments. Aliquots of approximately equal concentrations of $SOCl_2$ were achieved by using pulses of similar duration. For the very high humidity experiments, the

aliquot duration was increased somewhat due to the rapid consumption of the reactant during the initial stages of reaction. In addition to the more rapid decay at higher humidity, the high humidity traces also better illustrate the exponential nature of the $SOCl_2$ decay. Figure 6.4 also shows a very low humidity decay curve (RH 01%) where the $d[SOCl_2]/dt$ decay is seen to be very slow, with a half-life on the order of hours. In addition to the curves displayed in Figure 6.4, an additional experiment was carried out (not shown) where the tunnel was purged of all water down to the < tens of ppmV level. As expected, with little or no water, $d[SOCl_2]/dt \approx 0$, to within the noise level of the spectrometer.

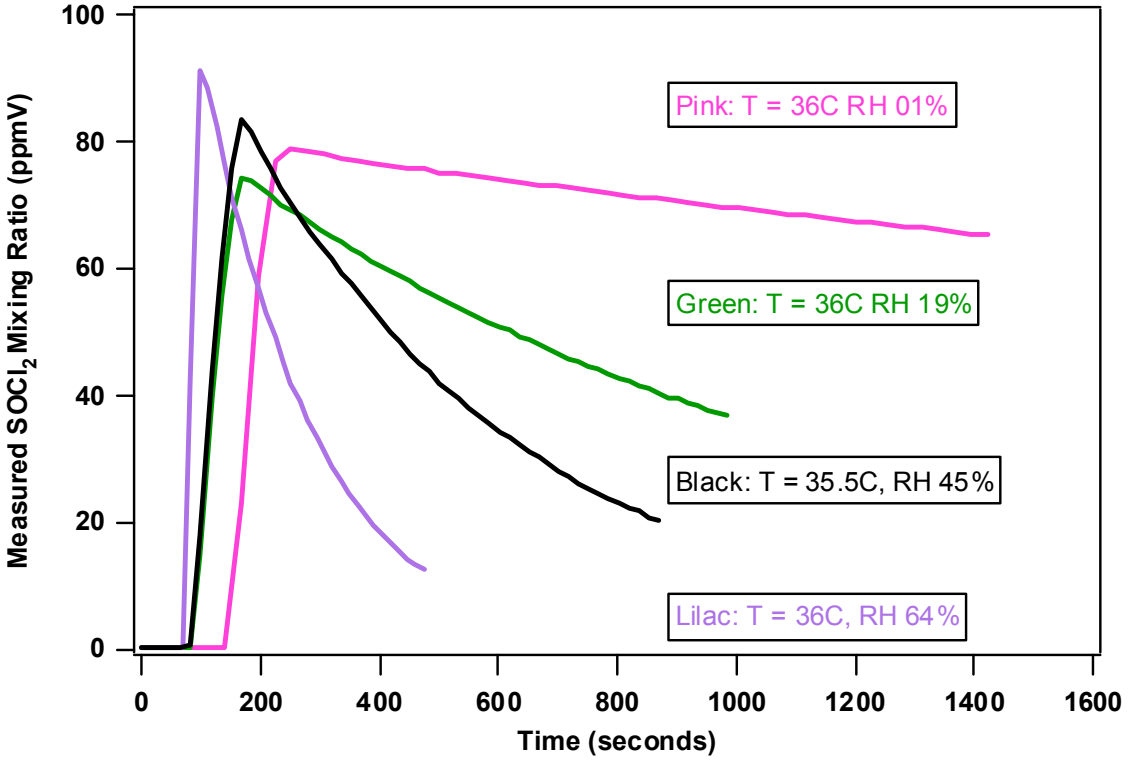

Figure 6.4. Multiple $SOCl_2$ decay curves as a function of relative humidity, all at ~36.5°C.

The thionyl chloride UV/Vis spectrum is displayed in Figure 6.5: $SOCl_2$ exhibited no absorbance in the range from 400 to 900 nm (i.e. it is colorless) and these data are therefore not plotted. The plot represents an average of four different measurements, the absorbance corresponding to 1 ppmV-m. The $SOCl_2$ exhibits two very strong bands in the ultraviolet with absorption maxima at 247 nm (40,500 cm^{-1}) and at $\lambda < 200$ nm. The lack of any strong absorption at wavelengths longer than 290 nm, however, is the observation of greater significance for the atmospheric fate of this species, because it shows that tropospheric photolysis is thus unlikely.

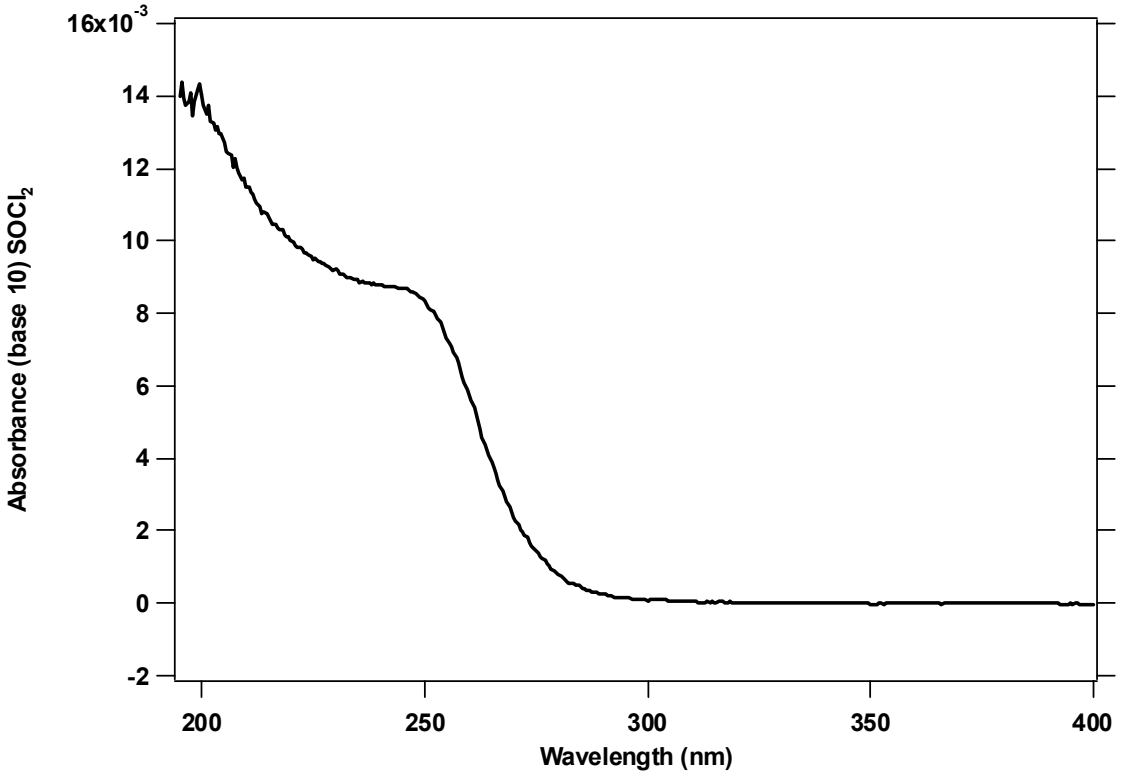

Figure 6.5. Ultraviolet/visible spectrum of $SOCl_2$ in the range from 400 to 190 nm. The molecule exhibited no absorbance between $900 < \lambda < 400$ nm and these data are not shown. The plot represents an average of four different absorption burdens.

6.5 Data Analysis

The $SOCl_2$ temporal plots contained in Figure 6.4 illustrate an important feature: The timescale for $SOCl_2$ concentration increase for all RH's is much shorter than the decay time. This allows the decay of $SOCl_2$ to be treated independently of the initial increase in $SOCl_2$ concentration. Based on this result, only two reactions will be assumed important in describing the decay of $SOCl_2$ in each experiment and are given as:

$$SOCl_2 + H_2O \rightarrow 2\,HCl + SO_2 \qquad (6.5)$$

$$SOCl_2 \rightarrow \text{Products} \qquad (6.6)$$

where reaction (6.5) is the homogeneous hydrolysis described by a (presumably) second-order rate coefficient k_h and reaction (6.6) is a first-order loss process used to characterize the reactive and non-reactive uptake of $SOCl_2$ onto the internal chamber surfaces (e.g. walls) described by k_w.

The general rate equation for the $SOCl_2$ hydrolysis is given by

$$d[SOCl_2]/dt = -k_h\,[SOCl_2]^a[H_2O]^b \qquad (6.7)$$

For these experiments clearly $[H_2O] >> [SOCl_2]$ and we can rewrite the rate equation as:

$$d[SOCl_2]/dt = -k' [SOCl_2]^a \quad (6.8)$$

where

$$k' = k_h [H_2O]^b \quad (6.9)$$

If the reaction is first-order in $SOCl_2$ then a = 1 and $\ln\left[\frac{SOCl_2(t)}{SOCl_2|_{t=0}}\right] = -k't$. Hence, we should observe a single exponential decay (Levine, 1983). For each of the 35 hydrolysis experiments, a single-exponential decay curve was fit to the measured data. For most of the experiments the decay curve was followed over one to two (1/e) lifetimes. The only exceptions to this were when the spectrometer noise level prevented obtaining accurate concentrations (for low $SOCl_2$ concentrations), or for the very low humidity experiments, e.g. 3% RH, where the decay time for an individual experiment would correspond to a significant fraction of a day. An example of one of the observed exponential decays along with the fit to a single exponential term (showing the reaction to be first order in $SOCl_2$) is shown in Figure 6.3. The raw data from four additional $SOCl_2$ decays at 36°C (showing the effect of RH) are presented in Figure 6.4. Although the fits are not all displayed in Figure 6.4, each of the thirty-five $SOCl_2$ decays was fit very well by a single exponential decay, thus showing a=1.

The order with respect to water is also clearly of interest. Since we have not one but many hydrolysis experiments, we can use the inverse of the decay lifetime $(1/\tau') = k'$ from each of the $SOCl_2$ decay curves, and take the logarithm of equation (6.9) to obtain

$$\ln (k') = \ln (k_h) + b \ln (H_2O). \quad (6.10)$$

Thus, if we use an entire set of decay curves such as those in Figure 6.4, each at a known different humidity and measured exponential decay constant k', a plot of ln (k') versus ln (H_2O) yields as slope the reaction order with respect to water, b. Figure 6.6 plots ln(k') versus ln(H_2O) for the 24°C (297 K) experiments and as can be seen from the plot, the agreement is good. The slope of the fit was determined to be b = 1.13 ± 0.14, meaning that, to within experimental error, the reaction is first order in water.

If we now take a = b = 1, the rate constant k_h for the overall hydrolysis rate expression (equation 6.7) can be obtained directly from any of the hydrolysis experiments by substituting the measured concentrations and reaction rate. For our data, the mixing ratios (in ppmV) had to first be converted to concentrations (molecules/cm^3) using the wind tunnel temperature and pressure for the given day/experiment. Using the fitted decay curves to determine the slope $d[SOCl_2]/dt$, the overall rate constant k_h was determined for each experiment by using equation (6.7) with both a and b taken as 1. For the 24°C (297 K) data we determined an average value of $k_{h(297)} = 5.0 \pm 1.3 \times 10^{-21}$ cm^3/(molecule-sec), which represents an average of 12 experimental decays, where we have intentionally discarded the experiments at low humidities (RH < 10%). The reasons for discarding the low RH data are twofold: First, the humidity sensor is quite unreliable at the low humidities, and the relative fractional error grows rapidly, for example, depending on whether the sensor displays either 2 or 3 % RH. Secondly, at the low humidities the $SOCl_2$ hydrolysis can have a half-life of several hours or more (e.g. see Figure 6.4) and as a consequence the present data do not follow the decay over even a single 1/e lifetime yielding less reliable single-exponential fits. For the 36°C (309 K) data k_h was determined to be $k_{h(309)} = 4.3 \pm 1.5 \times 10^{-21}$ cm^3/(molecule-sec) as derived from 8 measurements. The 10^{-21} cm^3/(molecule-sec) values are both plausible for an atmospheric bimolecular rate coefficient (Seinfeld and Pandis, 1998). Although the difference in rate constants for the two temperatures is not greater than the experimental uncertainty, the

decrease in rate coefficient at higher temperature may suggest a negative activation energy characterizes the reaction. If true, complex formation prior to reaction is consistent with the first order dependencies of both water and thionyl chloride. Obviously, further experiments are required to confirm this hypothesis.

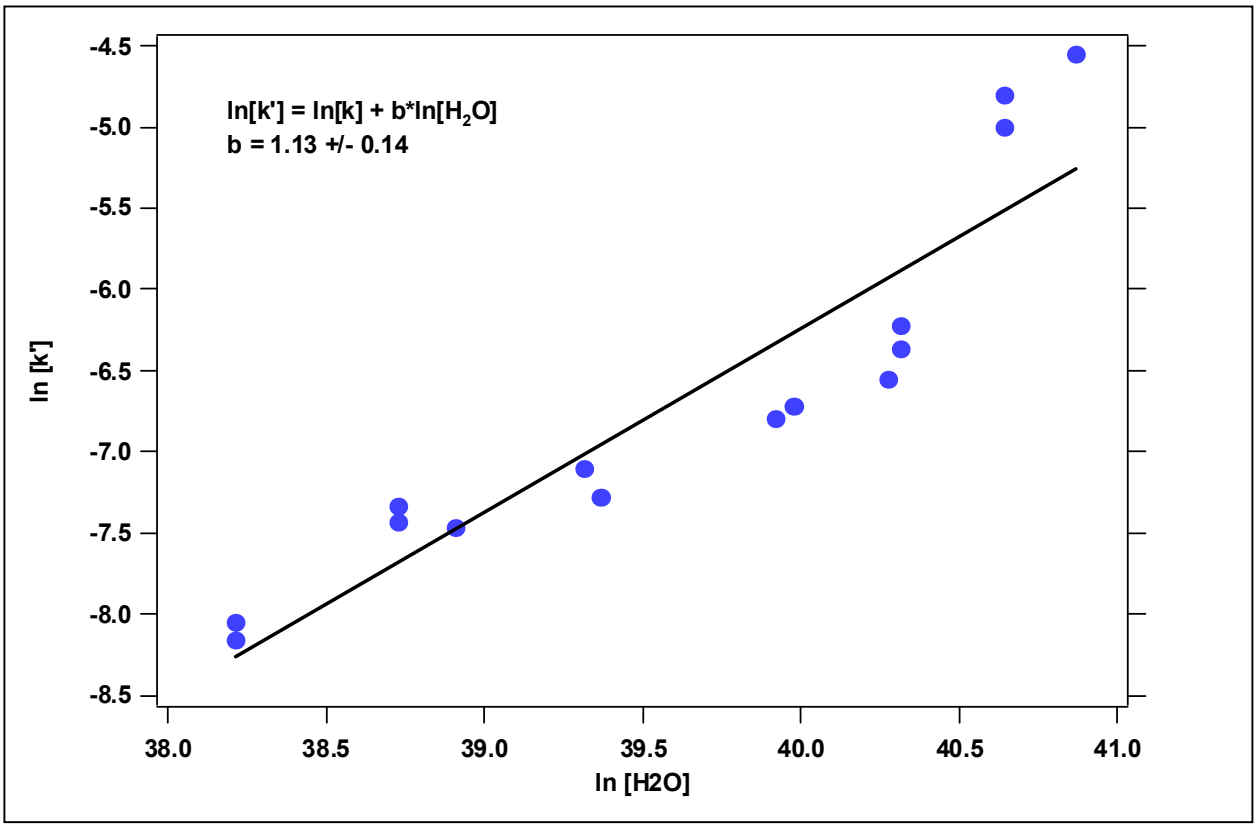

Figure 6.6. Plot of ln(k') versus ln(H_2O) for the series of multiple hydrolysis experiments at 24°C (297 K), each at a different humidity. k' (= $1/\tau_{obs}$) is the pseudo-first order rate constant for $SOCl_2$ decay where water is in excess. The slope, b, is the reaction order with respect to water.

6.6 Discussion

Our analysis has suggested, but does not prove, that the $SOCl_2$ hydrolysis may occur as part of an elementary reaction, perhaps as a single reactive complex. The observed pseudo-first order behavior seen for all the decay curves shows the homogenous hydrolysis reaction (6.5) to be first order in $SOCl_2$. The dependence on water was established by first observing that $SOCl_2$(g) decay does not proceed in the absence of water (see e.g. the RH 01% upper trace in Figure 6.4). The rate order in [H_2O] was determined (with less confidence than the rate order for $SOCl_2$) by using the decay constants from the hydrolysis at several different humidities to yield b=1. Although not irrefutable, there is further circumstantial evidence to support the homogeneous hydrolysis mechanism shown in equation (6.5), namely that the two products HCl(g) and SO_2(g) were formed in nearly 2:1 stoichiometric amounts, and that they were the only products observed by both the IR and GC/MS techniques. This certainly does not preclude a surface-catalyzed reaction between H_2O and $SOCl_2$, but the IR spectra showed both the SO_2 and HCl products were in the gas-phase.

However, if the SO_2 and HCl are direct products of the proposed hydrolysis reaction (2), then their stoichiometry should not only be 2:1 (as was observed within experimental error), but moreover their formation rates should match the decay rate of $SOCl_2$. This was indeed the case. If, in a given experiment, e.g. 25 ppmV of $SOCl_2$(g) was consumed over a certain time, 25 ppmV of SO_2(g) was formed. For the gas-phase HCl the agreement between 2 HCl formed for each 1 $SOCl_2$(g) consumed was not quite as good. The ratio was typically < 2 for HCl, presumably due to HCl's weak IR signal and due to the HCl adsorption problem discussed above.

In a seemingly analogous reaction between SO_3 and water vapor, recent work (Kolb *et al*. 1994, Jayne *et al*. 1997 and Lovejoy *et al*. 1996) established that the SO_3 reaction is second order in water vapor, though originally thought to be first order. Our data do not indicate this for the $SOCl_2$ hydrolysis, as the slope in Figure 6.5 is closer to 1, and the hydrolysis may indicate an apparent negative activation energy. Clearly more temperatures must be studied to make meaningful assertions as to the activation energy, and it would be well to try other techniques to further investigate the $SOCl_2$ hydrolysis such as the turbulent flow/CIMS technique (Kolb *et al*. 1994) or possibly using isotopically labeled species. Matrix isolation techniques have proven useful at isolating such intermediates (Tso and Lee, 1984) and recently step-scan FTIR has proven useful at elucidating intermediates for reactions that can be triggered in a reproducible manner (Letendre *et al*. 1999, Dattelbaum *et al*. 2002).

For typical boundary layer conditions of T = 298 K and 50% relative humidity, the 5.0×10^{-21} cm^3/molecule-sec rate constant corresponds to a 1/e lifetime of 514 s (8.6 min). Another conceivable loss process in the atmosphere could be reaction with the hydroxyl radical, OH. Assuming gas-kinetic limited reaction conditions of $k \sim 3 \times 10^{-12}$ cm^3/molecule sec, and a typical mid-latitude daytime tropospheric OH concentration of 5×10^6 molecules/cm^3 (Finlayson-Pitts and Pitts 1999) one obtains a theoretical $SOCl_2$ tropospheric lifetime due to OH reaction of 18.5 hours. These considerations reveal that hydrolysis, and not photolysis or reaction with OH, will be the dominant troposphere degradation pathway for $SOCl_2$ under typical ambient conditions. It should be noted that partial motivation for this work is to develop a database of hydrolysis rate coefficients for inorganic species so as to enable structure-activity relationships (SAR's) for inorganic compounds to be developed to the extent that they are for the oxidation of organic compounds.

7.0 Conclusions

As anticipated, no significant differences in the disappearance of pinacolyl alcohol from the wind tunnel atmosphere were observed by FTIR spectroscopy or gas chromatography under any of the conditions tested, indicating that as anticipated, temperature and relative humidity do not have a detectable influence on the degradation of gas-phase pinacolyl alcohol under the simulated transport scenarios. Exposure to simulated sunlight also did not affect alcohol concentration. However, the effective exposure time of the chemical to the UV light was determined to be less than needed to simulate near-field transport. Therefore, the system was modified (Figure 2.2) to lengthen the exposure time to simulated sunlight for the remaining test chemicals.

In the modified test system, photolysis of CH_3I was observed at a rate comparable to reported values for the type of lighting conditions tested. No changes were observed in CH_3I concentrations for those conditions that have been shown to result in a slow (relative to near-field transport) decay. Under the test conditions, methanol appeared to be a significant photolysis decay product when CH_3I concentrations are high. When ambient concentrations of the halomethane are low, quantification of the compound by FTIR spectroscopy is poor due to water vapor interference. However, because of the strong Q-branch of the 1250 cm^{-1} band, identification of the signature can still be accomplished.

These tests provided both negative and positive control scenarios to test the function of the test system for near-field fate tests. The subsequent tests of selected reactive chemicals (DCMP and $SOCl_2$) were performed using the modifications made during these tests. The atmospheric fates of DCMP and $SOCl_2$ were investigated in the semi-dynamic closed system under a variety of environmentally relevant temperature, humidity and lighting conditions. It was determined that humidity plays an important role, as water vapor reacts rapidly both with the methylphosphonic dichloride and with thionyl chloride.

DCMP hydrolysis formed HCl(g) and an (as yet) unidentified product(s) of the phosphorous moiety; the rapidity of their production was dependent upon the relative humidity of the atmosphere into which DCMP was introduced. Compound dissociation was so rapid at high relative humidity (≥80% RH) that sufficient concentrations of the parent chemical to permit determination of the decay rate could not be attained. The rate constant for hydrolysis at 296 K was determined to be $k_h = 6.0 \pm 1.9 \times 10^{-21}$ cm^3/(molecule-sec), resulting in a tropospheric lifetime on the order of only a few minutes due to hydrolysis.

$SOCl_2$'s near-field fate showed little effect due to oxidation or photolysis. However, $SOCl_2$ was found to rapidly hydrolyze to form SO_2(g) and HCl(g) in a nearly stoichiometric ratio of 2:1. From 24°C (297 K) data we determined an average value of $k_{h(297)} = 5.0 \pm 1.3 \times 10^{-21}$ cm^3/(molecule-sec), which represents an average of 12 experimental decays. For the 36°C (309 K) data k_h was determined to be $k_{h(309)} = 4.3 \pm 1.5 \times 10^{-21}$ cm^3/(molecule-sec) as derived from 8 measurements. For typical boundary layer conditions of T = 297 K and 50% relative humidity, the 5.0×10^{-21} cm^3/molecule-sec rate constant corresponds to a 1/e lifetime of 514 s (8.6 min). However, in desert climates, the humidity can be considerably lower and the lifetime correspondingly longer.

These results point to the need for reliable data that can indicate the atmospheric lifetimes, decay mechanisms and the breakdown pathways for molecules released to the atmosphere. Even simple

predictive capability is lacking, as structure-activity relationships have not been developed for many inorganic compounds due to the lack of kinetic data. These results specifically provide the first information on the kinetics of DCMP and $SOCl_2$ degradation that is applicable to near-field detection, in particular the rates of hydrolysis, and the importance of hydrolysis as compared to either OH-oxidation or photolysis.

The changes in near-source concentration and composition observed in this study further indicate that the utility of specific chemical signatures for source determination and monitoring must be evaluated against the background of local environmental conditions. Failure to do so may fail to identify pollution sources or underestimate production. In addition, more viable signatures of the polluting process may be obtained by investigating the near-field fate of process signatures, thus providing essential information for the development of contaminant detection systems. Also identified in this study is the potential usefulness of plant off-gassing for the detection of signature compounds during non-production periods. A potential remote sensing technique with great sensitivity for detecting trace amounts of methyl iodide was also discussed.

REFERENCES

Atkinson R. 1994. "Gas-phase tropospheric chemistry of organic compounds." Monograph #2, *J. Phys. Chem. Ref. Data.*

Benson, S. 1976. *Thermochemical Kinetics*. John Wiley & Sons, New York.

Bennett, J. H., Hill, A. C. and Gates, D. M. 1973 "Absorption of air pollutants by a standardized plant canopy". *J. Air Pollut. Control Assoc*. 23:203-206.

Bennett, J. H., Hill, A. C. and Gates, D. M. 1973 "A model for gaseous pollutant sorption by leaves". *J. Air Pollut. Control Assoc*. 23:952-957.

Bertie, J. E. 1998. "Specification of components, methods and parameters in Fourier Transform Spectroscopy by Michelson and related interferometers." *Pure and Appl. Chem*. 70 (10): 2039-2045.

Cataldo, D., P. Van Voris, M. Ligotke, R. Fellows, B. McVeety, S. Li, H. Bolton, Jr., and J. Frederickson. 1989. *Evaluate and Characterize Mechanisms controlling Transport, Fate, and Effects of Army Smokes in an Aerosol Wind Tunnel: Transport, Transport, Transformations, Fate and Terrestrial Ecological Effects of Fog Oil Obscurant Smokes*. AD-A20414. Pacific Northwest National Laboratory, Richland, Washington.

Chameides, W. L. and D. D. Davies. "Iodine-Its possible role in tropospheric photochemistry" 1980. *J. Geophys. Res*. C85: 7,383.

Chatfield, R. B., and P. J. Crutzen. 1990. "Are there interactions of iodine and sulfur species in marine air photochemistry?" *J. Geophys. Res*. 95(D13): 22,319 - 22,341.

Dahl, A. R., T.C. Marshall and C. H. Hobbs. 1984 "The acute toxicity of inhalable fluorophosponate (difluoro) and chlorophosphonate (dichloro) in three species of rodents." *Toxicologist* 4:22.

Dattelbaum, D. M.; Hartshorn, C. M.; Meyer, T. J. 2002. "Direct Measurement of Excited-state Intervalence Transfer in $[(tpy)Ru^{III}(tppz^{\bullet-})Ru^{II}(tpy)]^{4+*}$ by Time-resolved Near-infrared Spectroscopy", *J. Am. Chem. Soc*. 124, 4938-4939.

Finlayson-Pitts, B. J.; Pitts Jr., J. N. 1999. *Chemistry of the Upper and Lower Atmosphere*, Academic Press: New York.

Fried, A.; Sams, R; Berg, W. W. 1984. "Application of tunable diode laser absorption for trace stratospheric measurements of HCl: Laboratory results", *Applied Optics*, 23 (11): 1867-1880.

Griffith D.W.T. 1996. "Synthetic Calibration and Quantitative Analysis of Gas-Phase FT-IR Spectra", *Appl. Spectrosc*. 50:59-70.

Harris, G. W.; Klemp, D.; Zenker, T. 1992 "An upper limit on the HCl near-surface mixing ratio over the Atlantic measured using TDLAS", *J. Atmos. Chem*. 15:327-332.

Herzberg, G. 1945. *Molecular Spectra and Molecular Structure, II. Infrared and Raman Spectra of Polyatomic Molecules*, Van Nostrand Reinhold Co.: New York.

Jayne, J. T.; Pöschl, U.; Chen, Y.-M.; Dai, D.; Molina, L. T.; Worsnop, D. R.; Kolb, C. E.; Molina, M. J. 1997. "Pressure and Temperature Dependence of the Gas-Phase Reaction of SO_3 with H_2O and the Heterogeneous Reaction of SO_3 with H_2O/H_2SO_4 Surfaces", *J. Phys. Chem*. A 101, 10000-10011.

Johnson, T. J.; Sams, R. L., Blake, T. A., Sharpe, S. W., Chu, P. M. May 2002. "Removing aperture-induced artifacts from Fourier transform infrared intensity values", *Applied Optics* 41 (15), 2831-2839.

Johnson, T. J.; Disselkamp, R.S.; Su, Y-F; Fellows, R.J.; Alexander, M.L.; Driver, C.J. August 2002. "Gas Phase Hydrolysis of $SOCl_2$ at 297 and 309 K: Implications for Atmospheric Fate", Submitted to *J. Phys. Chem*.

Kelly, J. F. 2001, PNNL, personal communication.

Kolb, C. E.; Jayne, J. T.; Worsnop, D. R.; Molina, M. J.; Meads, R. F.; Viggiano, A. A. 1994. "Gas Phase Reaction of Sulfur Trioxide with Water Vapor", *J. Am. Chem. Soc*. 116 10314-10315.

Letendre, L. T.; Dai, H.-L.; McLaren, I. A.; Johnson, T.J. 1999. "Interfacing a Transient Digitizer to a Step-scan Fourier Transform Spectrometer for Nanosecond Time-resolved Spectroscopy", *Rev. Sci. Inst*. 70 18-22.

Levine, I. N. 1983. *Physical Chemistry, Second Edition*, McGraw-Hill, New York, Chapter 17.

Lovejoy, E. R.; Hanson, D. R.; Huey, L. G. 1996. "Kinetics and Products of the Gas-Phase Reaction of SO_3 with Water", *J. Phys. Chem*. 100 19,911-19,916.

Martin, P., E. C. Tuazon, R. Atkinson, and A. D. Maughan. 2002. Atmospheric gas-phase reactions of selected phosphorus-containing compounds. *J. Phys. Chem*. A 2002 106:1542-1550.

National Research Council (NRC) 1997. Fog Oil Smoke, In: *Toxicology of Military Smokes and Obscurants, Volume 1* . Committee on Toxicology, NRC and pp. 60-97, National Academy Press, Washington DC.

Neimysheva, A. A.; Knunyants, I. L. 1968. "Nucleophilic Substitution in a Series of Phosphorus Acid Derivatives. III Kinetics of the Hydrolysis of Phosphoric and Phosphonic Acid Dihalides", *Zh. Obshch.Khim*. 38(3) 595-601.

Riederer, M., 1995 "Partitioning and transport of organic chemicals between the atmospheric environment and leaves". *Plant contamination: Modeling and simulation of organic chemical processes*, pp. 153-190, Trapp S., McFarlane C. Eds. Lewis Publishers, Boca Raton Florida.

Probasco, K.M. A.D. Maughan, K.J. Pattison, R.S. Disselkamp, G.M. Gelston and F.C. Rutz. 2001. "Fate and Transport Analysis for the Recluse IA Site," Report Number *PNNL-13420*, Pacific Northwest National Laboratory, Richland, Washington.

Probasco, K.M. A.D. Maughan, K.J. Pattison, R.S. Disselkamp, G.M. Gelston and F.C. Rutz. 2001. "Fate and Transport Analysis for the Recluse MO Site," Report Number *PNNL-13494*, Pacific Northwest National Laboratory, Richland, Washington.

Roehl, C.M., J. B. Burkholder, G. K. Moortgat, A. R. Ravishankara, and P.J. Crutzen. 1997. "Temperature dependence of UV absorption cross sections and atmospheric implications of several alkyl iodides", *J. Geophys. Res*. 102(D11): 12,829.

Rosenblatt, D. H., S. M. Small, T. A. Kimmell and A.W. Anderson. 1995. "Agent Decontamination Chemistry: Technical Report, U. S. Army Test and Evaluation Command (TECOM) Technical Support, Phase 1." Prepared for the Environmental Quality Office, U. S. Army Test and Evaluation Command, by Argonne National Laboratory, Washington DC.

Seinfeld, J.H. and S.N. Pandis, 1998. *Atmospheric Chemistry and Physics: From Air Pollution to Climate Change*, John Wiley & Sons, Inc., New York, p. 247.

Sharpe, S.W. 2000. "Infrared Spectral Data Library", Report Number PNNL 11904-2, Pacific Northwest National Laboratory, Richland, Washington. http:://nwir.pnl.gov.

Sharpe, S. W.; Sams, R. L.; Johnson, T. J.; Chu, P. M.; Rhoderick, G. C.; Guenther, F. R. 2001. "Creation of 0.10 cm-1 resolution, quantitative, infrared spectral libraries for gas samples", *SPIE Proceedings in Environmental and Industrial Sensing*, 28 October – 2 November 2001, Newton, Massachusetts, USA, Conference 4577 Vibrational Spectroscopy-Based Sensor Systems, Paper number 4577-02.

Sumpf, B. 2001. "Line intensity and self-broadening investigations in the ν_1 and ν_3 bands of SO_2", *J. Mol. Struct*. 599:39-49.

Tso, T.-L.; Lee, E. K. C. 1984. "Formation of Sulfuric Acid and Sulfur Trioxide/Water Complex from Photooxidation of Hydrogen Sulfide in Solid O_2 at 15 K", *J. Phys. Chem*. 88, 2776-2781.

Warneck, P. 1988. *Chemistry of the Natural Atmosphere*, pp. 140 ff. Academic Press, New York.

Waschewsky G. C. G., R. Horansky, and V. Vaida. 1996. "Effect of dimers on the temperature-dependent absorption cross-section of methyl iodide," *J. Phys. Chem*. 100(24): 11559-11565.

Welke, B., Ettlinger K., Riederer M.; 1998 "Sorption of volatile organic chemicals in plant surfaces", *Environmental Science and Technology* 32 1099-1104.

Appendix A. Methanol Formation from Methyl Iodide

The formation of methanol is surprising. In general, most atmospheric mechanisms for the oxidation of methane or halomethanes result in the formation of formaldehyde, although the initial steps differ. For methane, the cycle begins with an attack by hydroxyl radical to form the methyl radical:

$$CH_4 + OH \rightarrow CH_3 + H_2O \quad (A.1)$$

For the halomethanes such as iodomethane, the chain begins with photolysis, but again the initial product is the methyl radical:

$$CH_3I + h\nu \rightarrow CH_3 + I \quad (A.2)$$

In either case the oxidation proceeds in a typical tropospheric environment as follows (Warneck 1988):

$$CH_3 + O_2 + M \rightarrow CH_3O_2 + M \quad (A.3)$$

$$CH_3O_2 + NO \rightarrow CH_3O + NO_2 \quad (A.4)$$

$$CH_3O + O_2 \rightarrow CH_2O + HO_2 \quad (A.5)$$

The formaldehyde formed in the last step (A.5) can undergo photolysis and/or reaction with OH eventually produces carbon monoxide (CO) as an oxidation product.

Generation of methanol, as seen in this study, may be a function of the relatively high initial concentration of CH_3I resulting from exposure to UV at 254 nm (below the 290 nm region, which is more typical of conditions found in the stratosphere. Photolysis of iodide largely occurs in the upper atmosphere where UV radiation is of sufficient energy to initiate a reaction; in the lower atmosphere photolysis of the compound is limited to the spectral region above 290 nm and, thus, would have much slower rates of decay (Roehl *et al*. 1997).

Methanol to Formaldehyde Ratio as Indicator of CH_3I

As we have discussed previously, the pertinent reactions for CH_3I photolysis can be approximated as:

A. $CH_3I + h\nu \rightarrow CH_3 + I$
B. $CH_3 + O_2 \rightarrow CH_3O_2$
C. $2\ CH_3O_2 \rightarrow 2\ CH_3O + O_2$
D. $CH_3O_2 + I \rightarrow CH_3O + IO$
E. $2\ IO \rightarrow I_2 + O_2$
F. $2\ CH_3O \rightarrow CH_3OH + HCHO$
G. $CH_3O + HCHO \rightarrow CH_3OH + HCO$
H. $HCO + O_2 \rightarrow HO_2 + CO$
I. $CH_3O + O_2 \rightarrow HCHO + HO_2$
J. $HO_2 + CH_3O \rightarrow CH_3OH + O_2$

K. $CO + CH_3O_2 \rightarrow CO_2 + CH_3O$ (? Rate coefficient not measured)
L. $HO_2 + CH_3O_2 \rightarrow O_2 + CH_3O_2H$ (methylhydroperoxide)

From the above reaction scenario, reaction (F) will initially yield equal amounts of methanol and formaldehyde. As the extent of reaction increases, however, reactions (G, I, and J) will begin to affect this ratio. For example, if reactions (G and J) are much faster than reaction (I), then the concentration of methanol will greatly exceed the formaldehyde concentration. Omitted here are possible iodine chemistries that may also affect this ratio. Due the complex nature of the chemistry, we expect that only an experimental measurement of the methanol-to-formaldehyde concentration ratio to reveal its actual value (i.e., modeling is too complex). In the real atmosphere, formaldehyde photolysis will change this ratio. Quoting Seinfeld and Pandis: "The lifetimes of HCHO resulting from photolysis and OH radical reaction are ~4 hours and 1.5 days, respectively, leading to an overall lifetime of ~3 hours for overhead sun conditions" (Seinfeld & Pandis, 1998). Since formaldehyde is "sticky" (e.g., readily adsorbs onto chamber walls) control experiments are needed to ensure that the observed HCHO concentration is not being undersampled in an experiment.

A mechanism that may explain the formation of methanol instead of formaldehyde when CH_3I was exposed to UV in the wind tunnel was proposed. The reaction sequence again begins with the methyl iodide photolysis (A.6) followed by generation of the methyl peroxy radical (A.7):

$$CH_3I + h\nu \rightarrow CH_3 + I \qquad (A.6)$$

$$CH_3 + O_2 + M \rightarrow CH_3O_2 + M \qquad (A.7)$$

However, the relatively high CH_3O_2 concentrations allow the self-reaction to produce the methoxy radical CH_3O which in turn undergoes a self-reaction:

$$2CH_3O_2 \rightarrow 2CH_3O + O_2 \qquad (A.8)$$

$$2CH_3O \rightarrow CH_2O + CH_3OH \qquad (A.9)$$

The enthalpies of reaction for these last two reactions are ($\Delta H_{rxn\text{-}298K}$) –6.4 and –81.0 kcal/mol, respectively (Benson 1976). Although the formaldehyde produced is nominally stable, it can also be attacked by either the hydroxy or methoxy radical, in the case of methoxy producing another methanol:

$$CH_3O + CH_2O \rightarrow CH_3OH + HCO \ (\Delta H = -16.5 \text{ kcal/mol}) \qquad (A.10)$$

$$HCO + O_2 \rightarrow HO_2 + CO \qquad (A.11)$$

Although this mechanism suggests CO production, any CO produced was below the detection limit in the current system. An additional mechanism that could explain this is the further consumption of the CO, converting the HO_2 via ozone into OH that could eventually oxidize CO to CO_2:

$$HO_2 + O_3 \rightarrow OH + O_2 \qquad (A.12)$$

$$HO + CO \rightarrow CO_2 + H \qquad (A.13)$$

$$H + O_2 + M \rightarrow HO_2 + M \qquad (A.14)$$

The abundance of ozone (needed in the above mechanism) would be plausible in this environment due to the UV driving the NO_2 photolysis process to form O_3. In any case, further studies would be needed to corroborate such a mechanism. In particular detection mechanisms such as luminol for NO_x as well as UV absorption for ozone detection would be advantageous.